R. A. Sperling[1], T. Liedl[1], S. Duhr[1], S. Kudera[1], M. Zanella[1], C.-A. J. Lin[1,2], W. H. Chang[2], D. Braun[1], W. J. Parak[1*]

Size determination of (bio-) conjugated water-soluble colloidal nanoparticles - a comparison of different techniques

[1]Center for Nanoscience, Ludwig Maximilians Universität, München, Germany
[2]Center for Nano Bioengineering and R&D Center for Membrane Technology, Chung Yuan Christian University, Taiwan, R.O.C.
[*] Corresponding author: Wolfgang.Parak@physik.uni-muenchen.de

Supporting Information[1]

I) Particle synthesis
I.1) Synthesis protocol for CdSe and CdSe/ZnS particles
I.2) Synthesis protocol for CdTe particles
I.3) Synthesis protocol for Au particles
I.4) Polymer coating to convert hydrophobic into hydrophilic particles
I.5) Gel filtration chromatography
I.6) Modification of the particle surface with polyethylene glycol (PEG)

II) Transmission electron microscopy (TEM) analysis of the particles
II.1) Description of the image analysis
II.2) Results of the TEM analysis

III) Gelelectrophoresis experiments

IV) Size exclusion chromatography (SEC) experiments

V) FCS experiments

VI) Thermophoresis experiments

VII) Comparison of different methods
VII.1) Introduction to the differences of the methods
VII.2) Comparison of our results with values from literature

VIII) References

---

[1] The idea of this Supporting Information is to provide the interested reader with a detailed account of the raw data measured. It is by far not meant to be read from the beginning until the end. In contrast, due to the index on this page the reader can access the piece of information that he/she is interested in. All important and relevant information is included in the main paper and this Supporting Information expands on further details to specific points. We have taken great care to describe here everything as detailed as possible, so that a documentation about all experimental and evaluation steps is given.

I) Particle synthesis

I.1) Synthesis protocol for CdSe and CdSe/ZnS particles

Chemicals: Tri-n-octylphosphine oxide (TOPO, 99%, #22.330-1), tri-n-octylphosphine (TOP, 90%, 11.785-4), hexadecylamine (HDA, 90%, #H7.40-8), nonanoic acid (97%, #N5502), CdO (99.99+%, #20.289-4), Se (99.99%, #22.986-5), diethylzinc (#40.602-3), hexamethyldisilthiane ((TMS)$_2$S, #28.313-4), octanoic acid (>99.5%, #15.375-3), octanethiol (98.5+%, #47.183-6), octylamine (99%, #O580-2) were purchased from Sigma-Aldrich. Tri-n-butylphosphine (TBP, 99%, #15-5800) was purchased from Strem. Dodecylphosphonic acid (DDPA, technical grade) was purchased from Polycarbon Industries. A stock solution of Se in TBP was prepared as 20%wt.

Synthesis of CdSe nanoparticles: The synthesis of CdSe nanoparticles was performed according to the procedure described by Reiss et al.[1]: 5.76 g HDA, 2.26 g TOPO, 2.20 g DDPA and 0.50 g CdO were mixed in a 50 mL flask. The powders were molten under nitrogen and then degassed for ca. 20 minutes at 130 °C. Under nitrogen, the solution was heated to 290 – 310 °C until the color of the solution changed from brownish to transparent. The solution should not reach a temperature higher than ca. 320 °C, as at this temperature HDA will evaporate. Once the solution was clear, 1 mL TBP was injected into the flask and the remaining undissolved CdO was removed from the walls of the flask by agitating the flask. The temperature was then stabilized at 270°C and 1.6 g of Se:TBP was injected rapidly into the solution. After ca. 1 minute the solution showed a light yellow color indicating the nucleation of CdSe particles. The reaction was allowed to proceed for 20 minutes, and then it was stopped by removing the heat-source. The particles as prepared by now could not be directly precipitated by methanol as they would be stuck in a polymer-gel that presumably forms out of the free surfactants (mainly DDPA). In other words, the particles would be trapped in a big amount of organic material. In order to obtain free particles the gel has to be removed, which will be described in the following. Unfortunately there is no procedure available which works always and there is no other way than "playing". We try to describe strategies to remove the gel to the best of our knowledge.

The general strategy to remove gel bound to the surface of the particles is to add nonanoic acid which prevents formation of chains of DDPA-molecules. DDPA has two binding sites for Cd, as well as Cd has two binding sites for DDPA. Apparently for steric reasons a Cd ion cannot saturate both bonds of the DDPA. Nonanoic acid in turn has only one binding site for Cd, thus (NNA)$_2$Cd is formed and the formation of the gel is suppressed. In practise, after the reaction was stopped the solution was cooled down to ca. 100°C and 3 mL of toluene and 5 mL of nonanoic acid were added to the flask and the product was precipitated rapidly by addition of methanol as soon as it had cooled down to below 40-50 °C. The precipitate was dissolved in 5-10 mL toluene. Apart from the approach described above, there are several slightly different approaches to extract the particles from the gel. Which of these approaches yields the best results depends on the nature of the sample and certainly also on the exact composition of the growth solution, i.e. on the type of impurity and thus ultimately on the producer of the individual compounds. Generally one should try to wash the sample as fast as possible after the reaction. On the other hand, the methanol for the precipitation should not be added at a too high temperature. All approaches used in our group involve the addition of a solvent such as toluene or chloroform, nonanoic acid, and the precipitation of the particles with methanol. In the easiest case, it is sufficient to simply add a considerable amount (5-10 mL) of nonanoic acid to the reaction solution when it has cooled down to ca. 100 °C and then precipitate the particles from

the solution. Additionally the solution can be kept at ca. 90 °C after the addition of the nonanoic acid until the precipitation (for ca. one hour). This approach bears the danger to destroy the size distribution of the sample. In most cases we observed an enlargement of the fluorescence peak, and even the appearance of a second fluorescence line. We could show that in the presence of nonanoic acid new CdSe-particles can nucleate even at that low temperature [2].

A second approach is to first precipitate the particles out of the growth solution by addition of methanol. In this case, a sufficient amount (ca. 5 mL) of toluene has to be added to the warm (ca. 80 °C) growth solution in order to prevent solidification of the organic material. Generally this yields a huge precipitate that is hard to dissolve in toluene. From this gel, the particles can be extracted by the addition of toluene and nonanoic acid in equal parts. By heavy agitation and eventual moderate heating of the sample the gel can be dispersed in the solvent. Subsequent centrifugation yields a precipitate of the same size as the first precipitate and a very clear supernatant that is now colored red, indicating the presence of nanoparticles. The supernatant can be transferred carefully to another vial. By repetition of this process more particles can be extracted from the gel. In this process it makes a difference if one uses toluene or chloroform. Toluene is lighter than the gel, thus in the centrifugation the gel is found as the lower phase. When chloroform is used, the lower phase is the clear gel-free phase, and therefore it is fairly difficult to extract this phase from the vial without polluting it with the gel.

In all cases, once a gel-free solution with free particles had been obtained, this had to be washed to remove the residual free reactants. To do so, the particles were precipitated twice by addition of methanol to the solution and subsequent re-dissolution in toluene. Methanol for the precipitation was added until the solution turned completely cloudy. Generally this was obtained when the ratio solvent-to-nonsolvent was roughly 1:1. When a shell growth on the CdSe-core is intended it is of advantage to dissolve the final sample in chloroform, as this solvent can be easily evaporated from the growth-solution for the shell-growth. At this point the CdSe cores are freely dispersed in chloroform. To characterize the samples absorption- and fluorescence-spectra, and transmission-electron microscopy (TEM) images were recorded. These data are shown in Figure SI-I.1.

Growth of a ZnS shell onto the CdSe particles: In order to increase the fluorescence intensity of the CdSe-nanoparticles, a shell of a different material is grown around the particles. This shell consists of the ZnS, which has a wider bandgap than CdSe and thus enhances the confinement of the exciton in the volume of the CdSe core. The synthesis is carried out according to the protocol described by Dabboussi et al. [3]. In detail, a typical protocol reads as follows: 6 g TOPO (technical grade, purchased from Sigma-Aldrich, #34.618-7) was molten and degassed at 130 °C. Then 1.5 mL TOP were added and ca. a sixth of the yield of the CdSe-synthesis was added in chloroform and the solution was degassed again to remove the chloroform. Then the particles were heated to 160 °C and a readily prepared stock-solution of Zn and S precursors (5.73 g TBP, 0.76 g diethylzinc, 0.22 g $(TMS)_2S$) was added dropwise to the particles. After each addition of 0.5 mL of stock solution the quantum yield of an aliquot was measured with respect to the initial bare CdSe-sample. The growth of the shell was stopped by cooling down the solution when the sample had just passed the maximum quantum yield. 5-10mL of butanol were added to prevent solidification of the TOPO. The sample was washed twice by repeated precipitation with methanol and subsequent re-dissolution in chloroform. At this point the CdSe/ZnS core/shell particles are freely dispersed in chloroform. To characterize the samples absorption- and fluorescence-spectra, and transmission-electron microscopy (TEM) images were recorded. These data are shown in Figure SI-I.1 and Table SI-I.1.
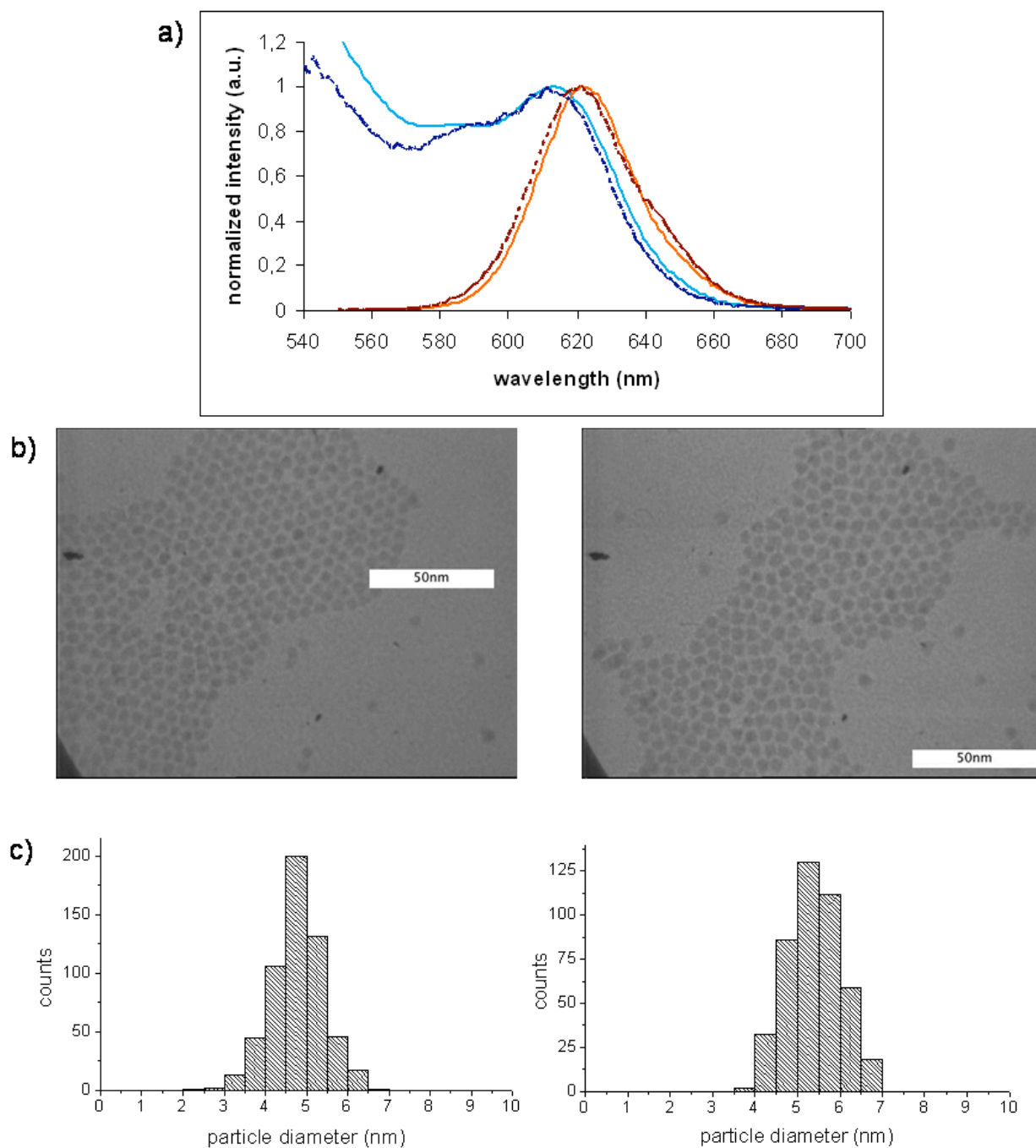
a)

b)

50nm

50nm

c)

Figure SI-I.1: Characterization of hydrophobic CdSe and CdSe/ZnS particles that are soluble in chloroform. a) Absorption (blue) and emission spectra (red) of CdSe (dark color) and CdSe/ZnS (light color) particles. The wavelengths of the absorption of the first excition peaks are 610 nm and 614 nm and the wavelengths of the maximum of the emission peak are 620 nm and 624 nm for CdSe and CdSe/ZnS particles, respectively. b) Transmission electron microscopy (TEM) images for CdSe (left) and CdSe/ZnS (right) particles. The scale bars correspond to 50 nm. c) Histograms of the size distribution of the diameter <d> of the inorganic CdSe (left, <d> = 4.7 nm) and CdSe/ZnS (right, <d> = 5.3 nm) particles as obtained from the TEM images.

I.2) Synthesis protocol for CdTe particles

Before the actual synthesis, a stock solution of Tellurium in tri-n-octylphosphine (TOP, 90% Sigma) was prepared: 1 g Te was mixed with 9 g TOP under nitrogen. In order to completely dissolve the Te, the mixture was heated to 200 °C for more than one hour. Residual undissolved Te was removed by centrifugation.

The synthesis was adapted from Yu et al. [4]. 3.70 g tri-n-octylphosphine oxide (TOPO, 99% Sigma), 0.270g octadecyl phosphonic acid (ODPA, Polycarbon Industries) and 0.051 g CdO (99.99+%, Sigma-Aldrich) were mixed in a 50 ml flask. The mixture was melted under nitrogen and degassed for ca. 20 minutes at 130 °C. The brown solution was then heated to above 340 °C under nitrogen until it turned transparent. To this clear solution, 1 mL of TOP was added. The temperature was then stabilized at 370 °C and the reaction was started by the fast injection 0.550 g of the Te:TOP solution. Nucleation was observed after ca. 10 seconds by a sudden darkening of the solution. The particles were allowed to grow for 90 seconds. The reaction was stopped by removing the heating mantle from the flask. When the solution had reached a temperature below 100 °C, 3 mL of anhydrous toluene was added to the solution to prevent solidification of the solvents. The solution was transferred to a glove-box and washed twice by repeated precipitation with anhydrous methanol and subsequent redissolution in toluene. The purified sample was dissolved in chloroform. At this point the CdTe core particles are freely dispersed in chloroform. To characterize the samples absorption- and fluorescence-spectra, and transmission-electron microscopy (TEM) images were recorded. These data are shown in Figure SI-I.2 and Table SI-I.1.

particle	λ_{abs} [nm]	λ_{em} [nm]
CdSe	610	620
CdSe/ZnS	614	624
CdTe	668	688

Table SI-I.1: Wavelength of the first exciton peak (λ_{abs}) in the absorption spectra and the corresponding wavelength of the maximum in the fluorescence emission (λ_{em}) for the CdSe, CdSe/ZnS, and CdTe particles that have been used in this study.
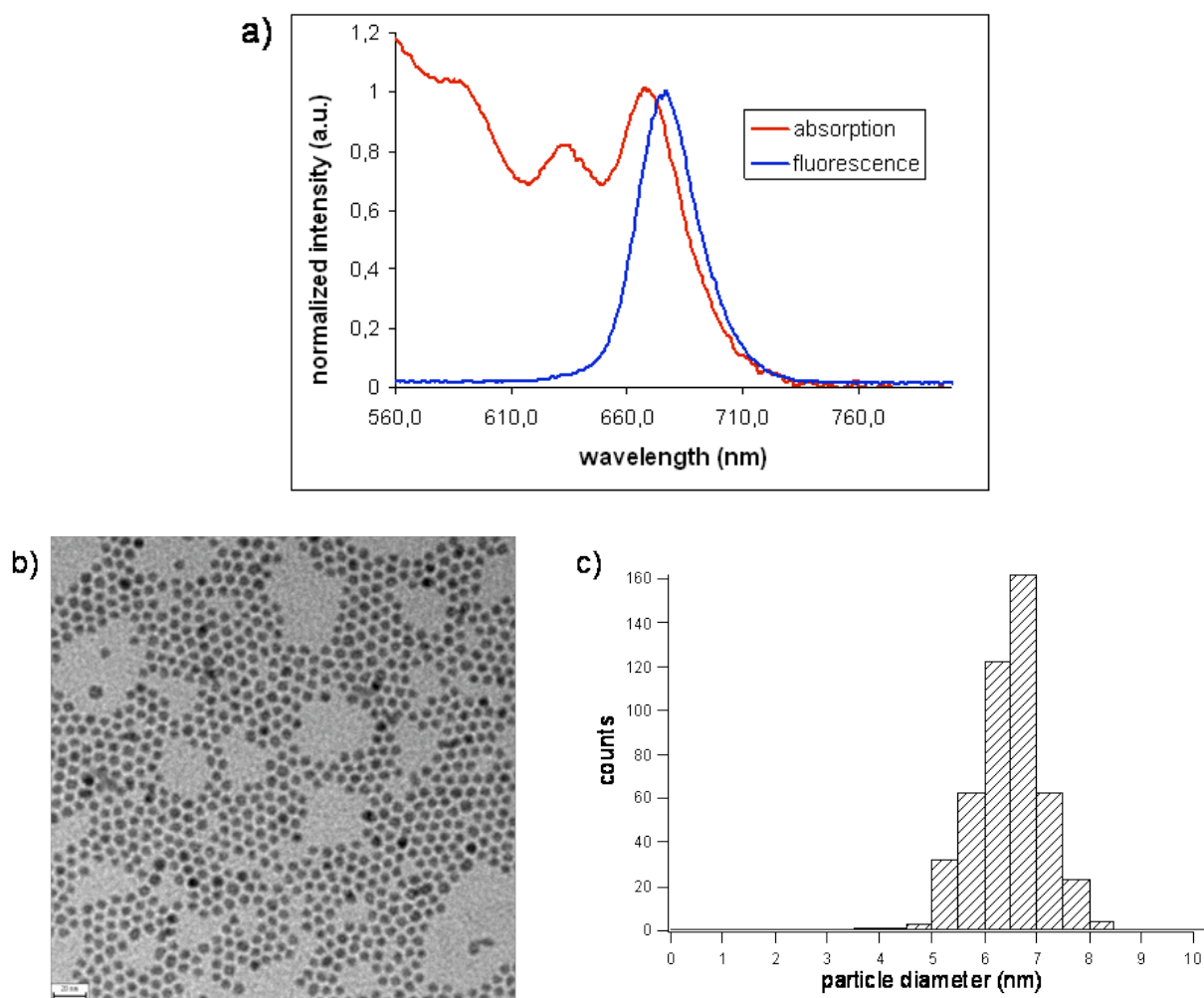
Figure SI-I.2: *Characterization of hydrophobic CdTe particles that are soluble in chloroform. a) absorption (blue) and emission spectra (red) of CdTe particles. The wavelength of the absorption of the first excition peak is 668 nm and the wavelength of the maximum of the emission peak is 677 nm. b) Transmission electron microscopy (TEM) image for CdTe particles. The scale bar corresponds to 20 nm. c) Histogram of the size distribution of the diameter <d> of the inorganic CdTe particles (<d> = 6.3 nm) as obtained from the TEM images.*

I.3) Synthesis protocol for Au particles

Colloidal Au nanocrystals were synthesized according to standard protocols [5,6]. The detailed procedure as used for the particles in this report is based on these initial publications and has been published in our previous manuscripts [7,8]. All glassware was carefully cleaned in a KOH/isopropanol bath and carefully rinsed with water before use. All reactions were carried out at room temperature under ambient conditions.

In a beaker, 2.17 g of tetraoctylammonium bromide ($(C_8H_{17})_4$NBr 98 %, Sigma-Aldrich #294136) were dissolved in 80 ml of HPLC grade toluene (C_6H_5Me) and transferred into a 250 ml separation funnel. 300 mg tetrachloroauric acid (hydrogen tetrachloroaurate (III): HAuCl$_4 \bullet x$H$_2$O 99.9 %, Alfa Aesar #12325) was weighted into a 20 ml vial, 25 ml Millipore water was added in three washing steps to yield a yellow translucent solution which was transferred to the separation funnel. The funnel was shaken for about 5 minutes in order to transfer the AuCl$_4^-$ ions into the organic phase. During this time the initially colorless toluene phase ("tol", on the top) turned dark red and the initially yellow aqueous phase ("aq", on the bottom) turned colorless, indicating the formation of tetraoctylammonium-gold ion pairs in the organic phase:

$$AuCl_4^-(aq) + N(C_8H_{17})_4^+(tol) \rightarrow N(C_8H_{17})_4^+ AuCl_4^- (tol)$$
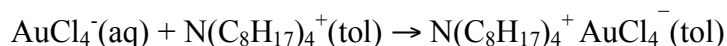
The aqueous phase was discarded and the toluene phase was transferred to a 250 ml round flask. In a beaker, 334 mg of sodium borohydride (NaBH$_4$ 98 %, Sigma-Aldrich #452882) was dissolved in 25 ml of Millipore water under vigorous stirring by means of a stirring magnet. The appearing small bubbles indicate the formation of hydrogen:

$$BH_4^- (aq) + 3H_2O \rightarrow B(OH)_3(aq) + 2H_2(\uparrow) + e^-$$
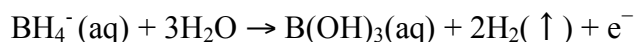
This clear solution was then pipetted dropwise within one minute into the red solution of tetraoctylammonium-gold in toluene. Upon stirring for few seconds, the color changed from red to red-violet. This color change indicates the nucleation of gold clusters mediated by sodium borohydride. The residual sodium borohydride in solution reduces the remaining gold ions, providing additional monomers for the growth of the nuclei

$$nAuCl_4^- (tol) + 3ne^- \rightarrow 4nCl^-(aq) + Au_n$$
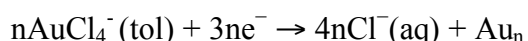
The Br$^-$ ions are supposed to be attached on the surface of the gold clusters, attracting again the N(C$_8$H$_{17}$)$_4^+$ counterions [6]. The solution was stirred for 1 hour, transferred to the cleaned separation funnel and 25 ml of 10 mM HCl were added in order to remove the excess sodium borohydride. The funnel was shaken for 1 minute and the aqueous phase on the bottom was discarded. 25 ml of 10 mM NaOH were added to the funnel to remove the excess acid and after shaking for 1 minute the aqueous phase was again discarded. Finally, 25 ml of Millipore water were added to remove excess ions, the funnel was shaken for 1 minute and the aqueous phase was discarded. This last washing step was repeated 2 more times. The aqueous phase and the eventually remaining emulsion were discarded. The organic phase was then transferred to a 100 ml round flask and stirred over night to allow the particles to Ostwald ripen to a thermodynamically stable average size and size distribution.

After the synthesis, a surfactant exchange procedure was carried out. For this, 10 ml of dodecanethiol ($C_{12}H_{25}$SH 98 %, Sigma-Aldrich #471364) were added to the Au nanocrystals in

toluene. The solution was heated to 65 °C and stirred for 2 – 3 hours. During this process the mercapto groups of the dodecanethiol molecules displace the Br⁻ and tetraoctylammonium ions and yield dodecanethiol capped Au nanocrystals. The solution was then cooled to room temperature and split into several half–filled 20 ml vials.

The Au nanocrystals were precipitated by the addition of about the same amount of methanol, followed by centrifugation for 2 min. After discarding the clear supernatant, the precipitate of each vial was dissolved in little toluene and these samples were pooled, yielding a total volume of 11 ml. This and the following precipitation steps removed the excess dodecanethiol molecules. The nanocrystals were then centrifuged for two minutes to precipitate larger aggregates, the supernatant was taken out and precipitated again by the addition of about 6 ml of methanol followed by centrifugation. The slightly colored supernatant was discarded and the precipitate was redissolved in 4 ml of toluene, yielding a solution of dodecanethiol capped Au particle with a concentration of usually 20 – 25 µM. The optical absorption spectrum, a TEM image and the size distribution of the particles are shown in Figure SI-1.3. The particle concentration was determined from the absorption at the plasmon peak (at around 515 nm) by using a molar extinction coefficient of $8.63 \cdot 10^6$ M^{-1}cm^{-1}. From the size-distribution of the TEM images a mean diameter of the inorganic Au-core of $<d> = 4.6$ nm was determined. (see Table SI-I.2).
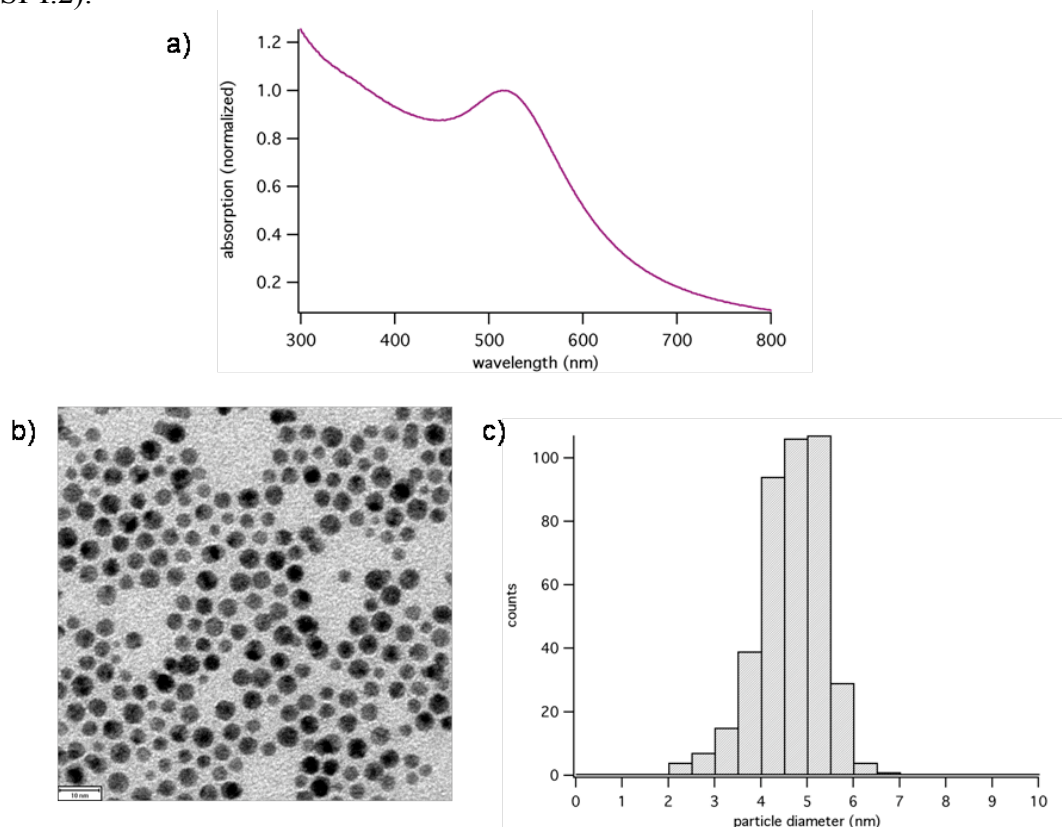

Figure SI-1.3: Characterization of hydrophobic Au particles that are soluble in chloroform. a) absorption spectra of Au particles. The wavelength of the plasmom peak is 515 nm. b) Transmission electron microscopy (TEM) image for Au particles. The scale bar corresponds to 10 nm. c) Histogram of the size distribution of the diameter <d> of the inorganic Au particles (<d> = 4.6 nm) as obtained from the TEM images.

I.4) Polymer coating to convert hydrophobic into hydrophilic particles

This protocol has been adapted from previously published reports [7,8]. As described therein, 100 monomer units of an amphiphilic polymer (poly(maleic anhydride alt-1-tetradecene), Sigma-Aldrich # 452513) and 10 crosslinker molecules (bis(hexamethylene)triamine, Sigma-Aldrich # 14506) were added per nm2 of the total surface A of the hydrophobically capped nanoparticles (as synthesized as described in Sections I.1 - I.3). For all particle samples, this total surface A of the particles was estimated by

$$A = V \, c \, N_A \cdot \frac{4}{3} \pi \, (r + r_{surf})^3$$

with the volume V of the particle solution, the particle concentration c, Avogardro's number N_A, the hardcore particle radius r and the length of the surfactant molecules r_{surf}. Besides the length of the surfactant molecules, that was assumed as $r_{surf} = 1.1$ nm for all particles[2], the inorganic core diameters were assumed for the different particle species as listed in Table SI-I.2.

	<d> (nm)	<r> (nm)	<r + r_surf> = <r_eff> (nm)	ε (cm⁻¹M⁻¹)
CdSe/ZnS	5.3	2.7	3.8	$4.79 \cdot 10^5$
CdTe	4.8	2.4	3.5	$2.79 \cdot 10^5$
Au	4.6	2.2	3.3	$8.63 \cdot 10^6$

Table SI-I.2: Diameters d, radii r, and extinction coefficients ε of the CdSe/ZnS, CdTe, and Au particles used in this study. <d> and <r> = <d>/2 always refer to the diameter and radius of the inorganic part of the nanoparticle, e.g. the CdSe/ZnS hardcore, the CdTe hardcore, and the Au hardcore. Actually the CdSe/ZnS hardcore is composed out of an inorganic CdSe core and an inorganic ZnS shell around it, but in this context we refer to the whole inorganic part as "core". The most straightforward way to determine <d> is to make TEM images of the particles and to measure the size of the inorganic particles from them (the organic surfactant shell does not give contrast and is thus invisible). For the particles used in this study the following values were obtained: CdSe/ZnS: <d>$_{TEM}$ = 5.3 nm (see Figure SI-I.1c), CdTe: <d>$_{TEM}$ = 6.3 nm (see Figure SI-I.2c), Au: <d>$_{TEM}$ = 4.6 nm (see Figure SI-I.3c). Since recording TEM images is some kind of laborious in general we derived the particles diameters not from TEM images, but either from the absorption spectra or by guessing. In the case of CdSe/ZnS and CdTe we typically derived the inorganic particle diameters by a calibration curve [9], in which the diameter of CdSe (!) and CdTe particles is listed versus the extinction coefficient of the particles at the first exciton peak. The values in this table for <d> have been obtained with this method: <d>$_{abs}$ = 5.4 nm for CdSe/ZnS and 4.8 nm for CdTe (see also Table SI-II.1). The described Au synthesis yielded typically particles with an inorganic diameter of <d> = 4.0 nm and we just assumed this value, also the actual value as measured by TEM can vary between different syntheses. Since the polymer coating procedure is relatively uncritical to the amounts of used polymer and crosslinker we therefore often use the guessed values, instead of measuring the actual values by TEM. The additional increase in radius due to the layer of organic surfactant molecules on the particle is roughly assumed to be r_{surf} = 1.1 nm, regardless of the actually used surfactant molecules. The effective particle diameter is the diameter of the inorganic core plus two times the thickness of the surfactant layer: <d$_{eff}$> = <d> + 2 r$_{surf}$. This corresponds to the effective particle diameter before (!) the polymer coating (see also Table SI-II.1).

---

[2] It has to be pointed out that for a refined model, the length of the surfactant can be estimated more precisely for the actual molecule, e.g. r_{surf}(dodecanethiol) ≈ 1.6 nm, r_{surf}(TOPO) ≈ 1.2 nm, and some correction for the geometric orientation of the molecules in respect to the particle surface. However, it was found that the polymer coating procedure is quite robust in regard to small changes, it worked well for all particles with the assumed value of r_{surf} = 1.1 nm.

For the polymer coating, all particles were dispersed in chloroform and the concentration was determined by the absorption spectra with the extinction coefficients from Table SI-I.2. Typically, the molar particle concentration of the stock solutions as used for the polymer coating was in the range of 5 – 20 μM. Of the polymer (poly(maleic anhydride alt-1-tetradecene, Sigma-Aldrich # 452513), a stock solution of 200 mM in regard of the monomer units (294.4 g/mol) in chloroform was prepared. The crosslinker (bis(hexamethylene)triamine, Sigma-Aldrich # 14506) was prepared as a 20 mM solution in chloroform.

The amount of polymer corresponding to 100 monomers/nm^2 was added to the nanoparticles in a round flask and the solvent was evaporated within 5 minutes at room temperature under reduced pressure. When the sample was dried, the amount of crosslinker corresponding to 10 molecules/nm^2 was diluted in some ml additional chloroform and added to the nanoparticles. The flask was shaken until all particles were redissolved in the solution, prior to the evaporation of the solvent within 5 minutes. The flask with the dried sample was vented and evacuated two times to assure that all solvent was evaporated[3]. Then, 10 – 20 ml of 50 mM sodium borate buffer pH 9 (SBB) or 0.5 x TBE (Sigma-Aldrich # T3919) was added and the flask was shaken until all solid had redissolved to yield a clear solution.

The nanoparticle solution was filtered through a syringe filter with a 0.22 μm CME membrane (Millipore, Roth #P818.1), and washed by diafiltration with SBB on Centriplus YM100 (Millipore # 4424) or Amicon-15 100k (Millipore # UFC910096) ultrafiltration devices.

Not all added polymer is wrapped around the particles. Some unbound polymer molecules can form polymer micells. These are stable assemblies of several (crosslinked) polymer molecules, in which the hydrophobic tails point towards the inside of the micell and the hydrophobic backbones are exposed to the outside, see Figure SI-I.4.
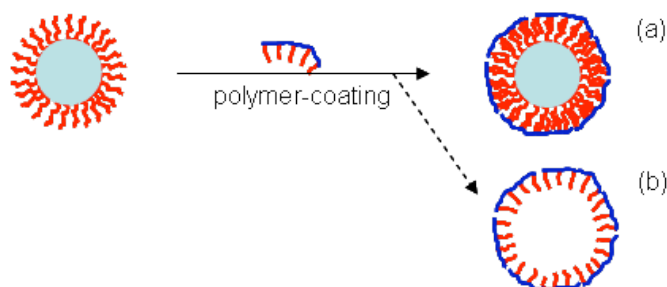

Figure SI-I.4: During the polymer coating procedure besides polymer coated particles (a) also polymer micells are formed (b). They can be thought as "empty" polymer shells without embedded inorganic particles. As the polymer shell around the particles also the micells are bound together by hydrophobic interaction. The hydrophobic tails of the amphiphilic polymer are drawn in red, the hydrophilic backbone in blue, the hydrophobic surfactant changes bound to the surface of the inorganic nanoparticle in red, and the nanoparticle in grey.

---

[3] The polymer coating did not work properly in case there was still some chloroform left.

I.5) Gel filtration chromatography

After the polymer-coating, the nanoparticles were routinely purified on a size exclusion gel filtration column (Sephacryl S-300 HR, GE Healthcare, #17-0599-10) connected to a standard HPLC system (Agilent 1100). The mobile phase was 50 mM sodium borate buffer with 100 mM NaCl, pH 9.0. The flow rate was set to 0.5 ml/min. The setup and the detailed procedure is described in Paragraph SI-IV. Usually, 1 ml of sample was injected in each run, the fractions containing the nanoparticles as observed by the absorption were collected and pooled, and the vials containing the front and tail fractions were discarded. Figure SI-I.5 shows examples of the elution profiles of CdSe/ZnS, CdTe, and Au particles directly after the polymer coating as described in Section I.4. The nanoparticles have a continuous absorption spectrum below their first exciton peak (for the semiconductors) and below their surface plasmon peak (for the gold), see Figures SI-I.1a, SI-I.2a, SI-I.3a. They therefore absorb in the visible close to their characteristic peak and in the UV range, while the polymer absorbs in the UV only. As mentioned in Section I.4 the polymer-coating procedure yields in addition to the polymer coated nanoparticles also some "empty" polymeric micells. Typically the polymer-coated nanoparticles are larger than the micelles of unbound polymer and therefore elute earlier on the size exclusion columns. In this way excess polymer (in the form of micells) can be separated from the polymer-coated particles. The solution containing the collected purified polymer-coated particles was diafiltrated three times with SBB pH 9 on Centriplus YM100 or Amicon 15 ultrafiltration devices to exchange the buffer and to concentrate the nanoparticles to a final concentration of 6.0 μM.
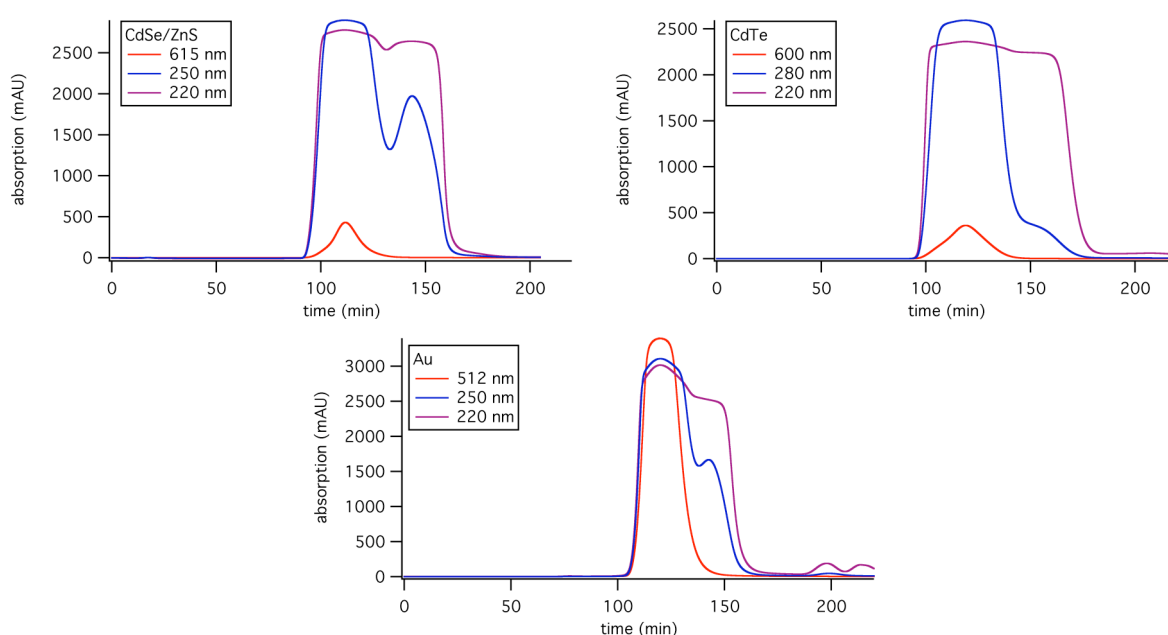

Figure SI-I.5: HPLC elution profiles of CdSe/ZnS, CdTe and Au nanoparticles after the polymer-coating. The absorption of the eluted samples is plotted versus the time. The bigger the particles are, the faster they pass the column and the earlier they are eluted. By the absorption at different wavelengths, the inorganic particle cores (absorbing in the visible and UV range) can be distinguished from the polymer (blue and purple lines, absorbing only in the UV at 250-280 nm and 220 nm). By stopping the sample collection at the end of the peak where only the inorganic cores absorb (red lines absorption in the visible at the characteristic absorption peak of the inorganic particles at 615 nm, 600 nm, 512 nm), most of the free polymer can be eliminated and only the purified polymer-coated nanoparticles are collected. The particles were run on a Sephacryl S-300 column at 0.5 ml/min with 50 mM sodium borate buffer with 100 mM NaCl, pH 9.0. Although the detector signal for the short wavelengths is saturated, a good separation of the particles from the free polymer could be observed.

I.6) Modification of the particle surface with polyethylene glycol (PEG)

Amino-modified PEG was attached to the carboxyl-groups present on the surface of polymer coated particles by EDC chemistry, see Figure SI-I.6. This protocol has been adjusted based on a previously published report [8]. Stock solutions of 3 mM methoxy-PEG-amine with a molecular weight of 750 g/mol (Sigma-Aldrich # 07964), 2000 g/mol (SunBio # P1AM-2), 5000 g/mol (Nektar Therapeutics # 2M2U0H01), 10000 g/mol (Sigma-Aldrich # 07965), and 20000 g/mol (Sigma-Aldrich # 07966) were prepared with by dissolving aliquots of some mg of PEG in sodium borate buffer (SBB) of pH 9.

Figure SI-I.6: *PEG molecules (drawn in green) are bound to the surface of polymer coated nanoparticles, in a way that 1, 2, 3 PEG molecules are bound per particle or that the particles surface is saturated with PEG.*

For CdSe/ZnS particles saturated with PEG, to 70 µl of the 6 µM particle solution 70 µl of the 3 mM PEG was added, resulting in a ratio of 500 PEG molecules per nanoparticle. Then, 70 µl of a fresh EDC solution (Sigma-Aldrich # E7750, 384 mM in SBB) was added, yielding a ratio of 64000 EDC molecules per nanoparticle and a final particle concentration of 2 µM in the reaction mixture. The samples were allowed to react 3 h before they were diafiltrated once with SBB on Centricon YM100 ultrafiltration devices.

For CdSe/ZnS particles with a defined number of attached molecules, 100 µl of a 3 mM PEG solution (M_W 5000 g/mol, 10000 g/mol, and 20000 g/mol) were added to 100 µl of 6 µM nanoparticles, yielding a ratio of 500 PEG molecules/nanoparticle. The ratio of EDC molecules per nanoparticle was experimentally determined by preparing a test-series with variable EDC concentration and running these particles on an agarose gel [8]. For the following reactions the EDC concentration at which discrete bands on gel of the test-series appeared was used. It has to be noted that the efficiency of the coupling reaction appears to be slightly higher at larger reaction volumes. For the CdSe/ZnS samples described here, 100 µl of a 1.74 mM solution of EDC in SBB was added to the nanoparticles with PEG, resulting in a ratio of 100 EDC molecules per nanoparticle. After allowing the mixture to react at least for 3 h, the samples were run on a 1 % agarose gel (Invitrogen #15510027) in 0.5 x TBE buffer (Sigma-Aldrich, # T3913) for typically 60 – 120 min at 100 V. The separation of the individual bands was controlled with an UV hand lamp before they were cut out by means of a scalpel. The gel cubes containing the bands were cut into smaller pieces and immersed in 50 mM SBB of pH 9 over night to 3 days. In this time the particles diffused out of the gel into solution. It was found that the fluorescence of the particles was reduced significantly or even totally when the extraction was carried out in 0.5 x TBE buffer. The samples were then concentrated to < 1 ml on Centricon YM100 ultrafiltration devices (Millipore) and desalted on NAP-25 columns (GE Healthcare, #17-0852-02) equilibrated with MilliQ water, while the elution was observed under illumination with an UV hand lamp. The attachment of PEG to Au particles was carried out in the same way for CdSe/ZnS particles, but instead of cutting out the bands the samples were only run on a 2 % agarose gel in order to derive the effective radii of particles with a discrete number of PEG molecules.

II) Transmission electron microscopy (TEM) analysis of the particles

II.1) Description of the image analysis

When nanoparticles are deposited on a surface, as for instance on a TEM-grid, the particles tend to form a 2D-lattice. By looking closer, one can observe that two neighboring particles do not touch each other, but leave a gap between them, see for example Figures SI-I.1b and SI-I.2b. This gap can be interpreted as the contribution of the organic surfactants that are adsorbed to the inorganic particle surface to the effective particle diameter, which consist of the inorganic particle core plus the surfactant layer. The surfactants consist mainly of alkyl-chains and therefore show only a very low contrast in the TEM.

The purpose of the image analysis as described here is to determine the thickness of the gap and in this way to determine the thickness of the surfactant layer. In order to do so, we measure the distance between the centers of two adjacent particles and subtract the diameter of a single particle. In this work this has been done by comparing different statistics. The diameter has been measured on about 500 individual particles and the results are reported in the histograms in Figure SI-I.1c and SI-I.2c. The distance between two particles has been determined with an automated image-analysis routine, which is described in the following paragraph. As it simply calculates the distance between all particles on one image, in the statistics (see Figures SI-II.2 and SI-II.3b) we find a peak not only for the first neighbors but also one combined peak for the second and third neighbors and some higher orders (not shown).

In order to determine the centers of the particles, one cannot just use the standard particle-analysis routine delivered with most analysis programs (as for instance Igor Pro (Wavemetrics) or ImageJ (NIH)). The general procedure for this type of analysis is to first transform the image into a binary image by reducing the color-range of each pixel to just black or white. In order to do so, a threshold is set. All pixels that have a grey value darker than this threshold are counted as black, the others as white. In a second step all closed areas of one of the two colors are marked as a particle. Applying this procedure to our TEM-images yields a quite faulty result, as frequently two adjacent particles are recognized as just one particle. The gap between two particles is usually not perfectly white, but has a grey-value only slightly different from that of the particles. Therefore the setting of the threshold always leads to a trade-off between erroneous connection of particles and an incomplete recognition of only the darkest particles.

To recognize the particles with a higher efficiency, we introduced a preprocessing step. We applied a Gaussian convolution-filter. This can be understood as a pattern search for circular structures. As a result, ideally we obtain very sharp and intense peaks as the positions of the centers of the particles. After this treatment the image analysis yields better results. The improvement is twice. First, adjacent particles, which show only little contrast in the gap are identified as separate particles and second fluctuations in the background are not identified as particles. This is demonstrated in the Figure SI-II.1.
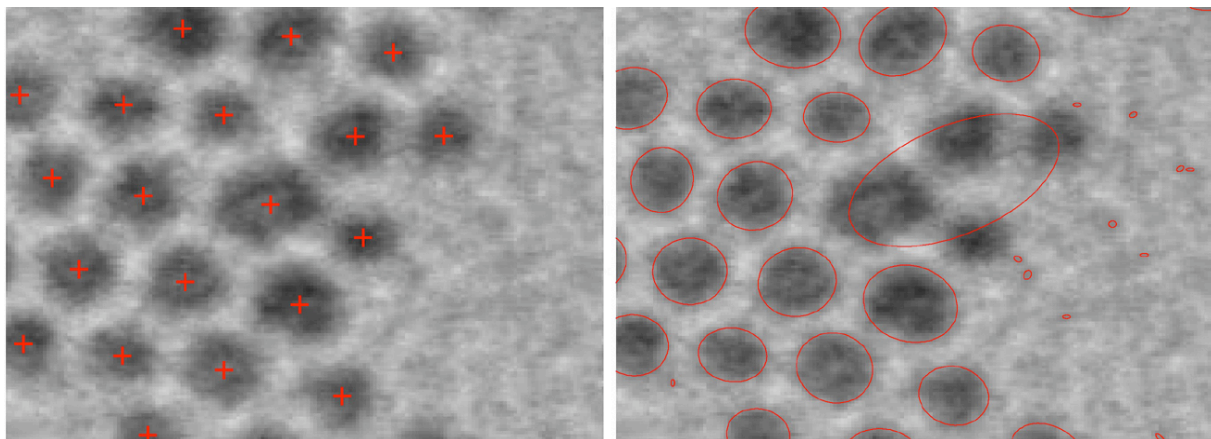
Figure SI-II.1: Demonstration of the improved particles analysis. The left panel shows the recognized centers of the particles with a cross mark. In this case a preprocessing step has been applied. In the right panel only the standard procedure was used. The particle areas are marked with red ellipses. In this case some adjacent particles are recognized as one and also some tiny spots are falsely identified as particles.

II.2) Results of the TEM analysis

The mean diameter of the inorganic part of the CdSe and CdSe/ZnS particles was directly extracted as $<d>_{TEM}$ = 4.7 nm and 5.3 nm from the TEM images as maximum in the histogram of the diameter distribution, see Figure SI-II.2. Yu et al. [9] have published a calibration curve which relates the wavelength of the first exciton peak to the diameter of the particle core. Absorption at 610 nm and 614 nm corresponds to a diameter of $<d>_{abs}$ = 5.1 nm and 5.3 nm for CdSe and CdSe/ZnS particles, respectively (the table actually has been made for CdSe particles; however, as first approximation we used the same table for CdSe/ZnS particles). Thus the resultant diameters from Yu et al. correspond well to our own data. All data are enlisted in Table SI-II.1.

The surfaces of two adjacent particles cannot get closer than two times the thickness of the organic shell around the inorganic particles. In Figure SI-II.2 the distribution of the distances of the centers of all particles are given for hydrophobic CdSe and CdSe/ZnS particles. The first maximum corresponds to two times the particle radius plus twice the thickness of the organic layer on the particle surface, which gives a number for the effective particle diameter $<d_{eff}>_{TEM}$ that comprises both, the inorganic and organic part. Since TEM images need to be recorded with dried particles these values have to be interpreted as lower limits. For the hydrophobic particles the effective diameter is around $<d_{eff}>_{TEM}$ = 6.0 nm and 6.4 nm for CdSe and CdSe/ZnS particles, respectively, see also Table SI-II.1. This corresponds to a thickness of the organic layer (that mainly consists out of trioctylphosphine oxide (TOPO) and hexadecylamine (HDA) molecules) of $(<d_{eff}> - <d>)_{TEM}$ / 2 = (6.0 nm - 4.7 nm) / 2 = 0.7 nm in the case of CdSe and $(<d_{eff}> - <d>)_{TEM}$ / 2 = (6.4 nm - 5.3 nm) / 2 = 0.6 nm in the case of CdSe/ZnS. This value lies in the expected range of the length of TOPO and HDA molecules. As mentioned above, the measured distance will be certainly underestimated.

Unfortunately we did not have a sufficient amount of CdSe/ZnS particles left to finish all TEM experiments (for all experiments with all different methods the same batch of CdSe/ZnS was used). Therefore for the analysis of polymer-coated particles we had to use a different batch of particles. It is very laborious to obtain two batches of CdSe/ZnS with the same properties. Since CdTe particles can be synthesized with a more regular spherical shape we used them for the determination of the thickness of the polymer shell. The surface chemistry of hydrophobically capped CdTe and CdSe/ZnS is very similar. We are aware that for this reason the obtained values have to be related with care to the data obtained with CdSe/ZnS. The following analysis about the thickness of the polymer layer is performed on CdTe and not on CdSe/ZnS.
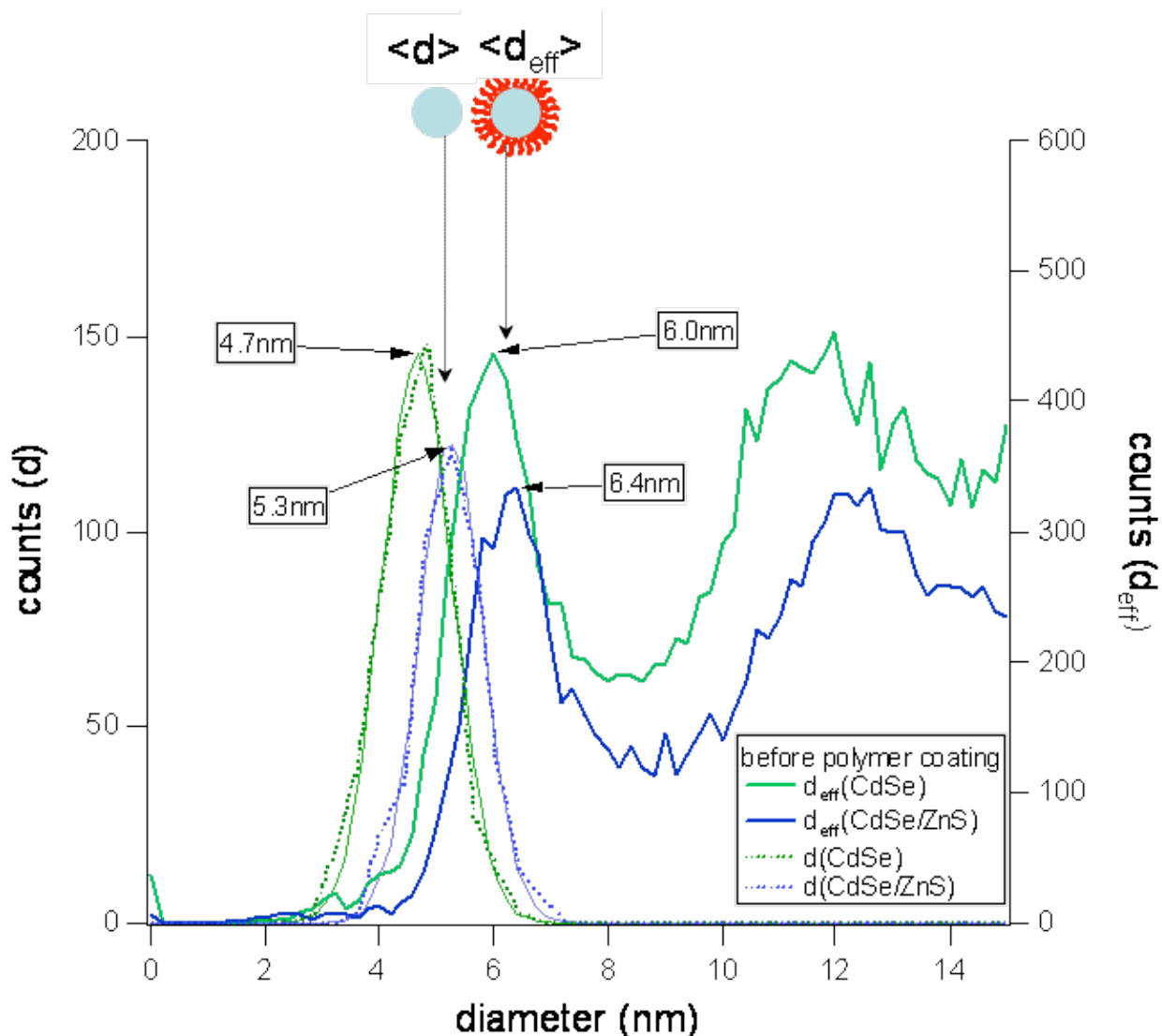
Figure SI-II.2: *The inorganic particle core (CdSe or CdSe/ZnS gray) of the hydrophobic particles is stabilized by surfactant molecules (red). On the left side graphics a histograms of the particle diameters d that have been measured from many TEM images and a fits to the histograms are shown. The data are plotted in green and blue for CdSe and CdSe/ZnS particles, respectively. The fits of the histograms (thin, solid lines) peak at $<d>_{TEM}$ = 4.7 nm and 5.3 nm for CdSe and CdSe/ZnS, respectively. This can be interpreted as the mean diameter of the inorganic part of the CdSe and CdSe/ZnS particles. The graph also contains the distribution of the distances between the centers of the particles for hydrophobic particles. The first peak in this distribution function can be interpreted as lower limit for effective particle diameter $<d_{eff}>_{TEM}$, i.e. the diameter of the inorganic particle plus the organic shell around the particle.*

The mean diameter of the inorganic part of the CdTe particles was directly extracted as $<d>_{TEM}$ = 6.3 nm from the TEM images as maximum in the histogram of the diameter distribution, see Figure SI-II.3. This is somehow different to the value of $<d>$ = 4.8 nm from a calibration curve reported by Yu et al. [9] that correlates the wavelength of the first exciton peak to particle diameters. We have double checked this by using two synthesis and analyses involving different persons and transmission electron microscopes. Therefore the Yu data seem not to be valid for all types of CdTe synthesis. On samples produced at different times, the correlation was quite reliable.
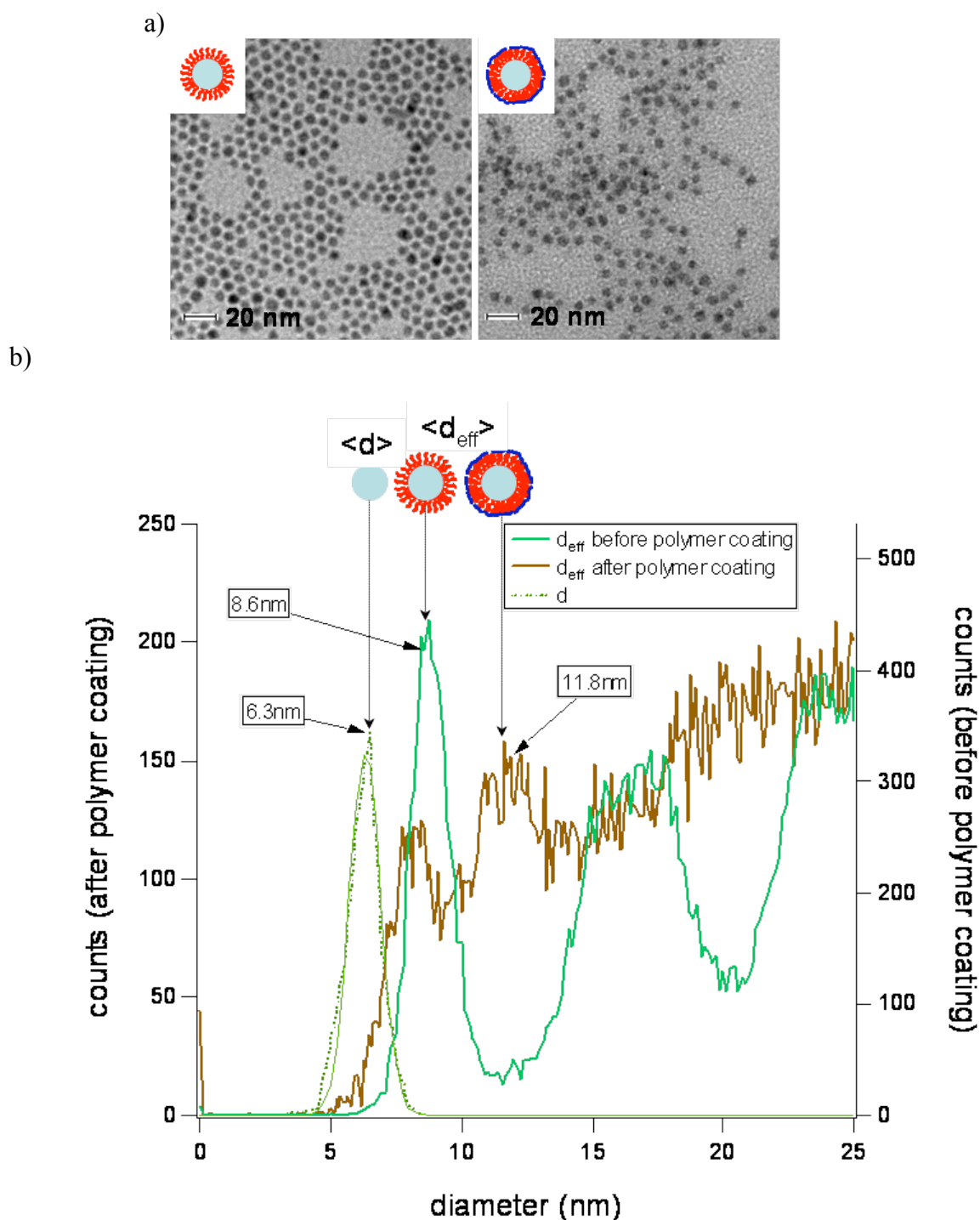
16

Figure SI-II.3: a) TEM images of hydrophobic and hydrophilic CdTe particles are shown on the left and right side, respectively. The inorganic particle core (gray) of the hydrophobic particles is stabilized by surfactant molecules (red). The hydrophilic particles have an additional amphiphilic polymer shell wrapped around the particle, whereby the hydrophobic side chains are drawn in red and the hydrophilic backbone in blue [7]. b) On the left side of the graphics a histogram of the particle diameters d that have been measured from many TEM images and a fit to the histogram is shown. The fit of the histogram peaks at $<d> = 6.3$ nm (as well for hydrophobic as for hydrophilic particles), which can be interpreted as the mean diameter of the inorganic part of the CdTe particles. The graph also contains the distribution of the distances between the centers of the particles for hydrophobic (green) and hydrophilic (brown) particles. The first peak in this distribution function can be interpreted as lower limit for effective particle diameter $<d_{eff}>_{TEM}$, i.e. the diameter of the inorganic CdTe particle plus the organic shell around the particle. In the case of hydrophobic particles the organic shell corresponds to the TOPO layer ($<d_{eff}>_{TEM} = 8.6$ nm), in the case of hydrophilic particles to the TOPO layer plus the amphiphilic polymer around it ($<d_{eff}>_{TEM} = 11.8$ nm).

17

In Figure SI-II.3b the distribution of the distances of the centers of all particles are given. The first maximum corresponds to two times the particle radius plus twice the thickness of the organic layer on the particle surface, which gives a number for the effective particle diameter $<d_{eff}>_{TEM}$ comprising both the inorganic and organic part. Since TEM images need to be recorded with dried particles these values have to be interpreted as lower limits. For the hydrophobic particles the effective diameter is around $<d_{eff}>_{TEM}$ = 8.6 nm. This corresponds to a thickness of the organic layer (that mainly consists out of trioctylphosphine oxide (TOPO) molecules) of $(<d_{eff}> - <d>)_{TEM}$ / 2 = (8.6 nm - 6.3 nm) / 2 = 1.2 nm, see Table SI-II.2. This value lies in the expected range of the length of TOPO molecules. As mentioned above the measured distance is certainly underestimated. For the hydrophilic particles the peaks in the distance distribution function are less pronounced. The first peak can be found at the same position as for the hydrophobic particles. There is a second peak at around 11.8 nm, which is not present for the hydrophobic particles. The first peak in the distribution of distances could be attributed to particles that are only partly coated by the polymer and the second peak could be attributed to particles that are completely coated with polymer. In this way the thickness of the organic layer (TOPO + polymer) would be estimated as $(<d_{eff}> - <d>)_{TEM}$ / 2 = (11.8 nm – 6.3 nm) / 2 = 2.8 nm, see Table SI-II.2. This suggests that in the dried state the additional increase in particle radius due to the polymer layer is around 2.8 nm - 1.2 nm = 1.6 nm. However, the arrangement of the hydrophilic particles on the TEM grid is much less regular than the one of the hydrophobic ones. The reduced ability of the polymer coated particles to arrange in a 2D-lattice might be due to several facts. First, the softness of their shell might lead to variable distances. Second, more than two particles might be wrapped in within the same polymer-shell. However, the results obtained with gel electrophoresis show that this cannot be a dominant process. Third, one might assume that the polymer coating is not very homogeneous and the broad distance distribution might result from the fact, that the polymer is not wrapped as nicely around the particles as assumed [7]. We assume this third possibility to be the most likely one. The data are compared in Table SI-II.1.

particle	$<d>_{TEM}$ [nm]	$<d>_{abs}$ [nm]	$<d_{eff}>_{TEM}$ [nm] (before polymer coating)	$<d_{eff}>_{TEM}$ [nm] (after polymer coating)
CdSe	4.7	5.1	6.0	-
CdSe/ZnS	5.3	5.3	6.4	-
CdTe	6.3	4.8	8.6	11.8
Au[4]	3.9	-	4.9	8.6

Table SI-II.1: Diameters of different particles. $<d>_{TEM}$ is the mean diameter of the inorganic part as determined from the histograms of the diameter distribution from TEM images. $<d>_{abs}$ corresponds to the mean diameter of the inorganic part as derived from the absorption spectra using a calibration curve in case of the semiconductor particles. This calibration curve created by Yu et al. [9] relates the wavelength of the first excition peak in the absorption spectra to a diameter (that had been also determined by TEM). The effective particle diameters were obtained as the mean distance between the centers of adjacent particles. The effective diameters $<d_{eff}>_{TEM}$ comprise the inorganic core of the particles plus the organic layer adsorbed to it. These values were obtained before and after the polymer coating.

---

[4] As in the case of Au particle the diameter of the Au core changed due to the fractioning process during the size exclusion chromatography purification from 4.6 nm to 3.9 nm in this table the effective before the polymer coating is referred to the core diameter of the hydrophilic cores. This means 0.7 nm have been subtracted from the effective diameter before polymer coating (as this refers to cores that are 0.7 nm bigger in diameter): 5.6 nm - 0.7 nm = 4.9 nm.

Unfortunately as described above because of running out of sample we were not able to determine with TEM the effective diameter of polymer coated CdSe/ZnS particles from the batch that has been used for all the rest of the experiments. Therefore, we decided to make a rough approximation. The thickness of the polymer layer in case of the CdTe particles has been estimated to 1.6 nm as described above. In first approximation we assume that this should be similar for CdSe/ZnS particles. Since the diameter of hydrophobic CdSe/ZnS particles (before polymer coating) is 6.4 nm we assume the diameter of hydrophilic CdSe/ZnS particles (after polymer coating) to be $<d_{eff}>_{TEM}$ (CdSe/ZnS after polymer coating) = 6.4 nm + 2× 1.6 nm = 9.6 nm. We have used this value in the main part of the paper. As already mentioned this has to be understood as a rough approximation. However, since the effective diameters obtained from the TEM experiments can be questioned at any rate because they were measured on dry samples and the data sets also do not shown unequivocally interpretable peaks, we are convinced that this approximation does not reduce the value of the presented work.

The same analysis as described above for CdSe/ZnS and CdTe particles was also applied to Au particles. Gold particles either capped with dodecanethiol (i.e. hydrophobic) or coated with an additional amphiphilic polymer shell (i.e. hydrophilic) were studied by TEM. Figure SI-II.4 shows the histograms of the Au core diameters d_{TEM} and the distribution of the distances between the centers of the particles for hydrophobic and hydrophilic particles. The first peak in this distribution function can be interpreted as lower limit for the effective particle diameter $<d_{eff}>_{TEM}$, i.e. the diameter of the inorganic Au core plus the organic shell around the particle. In the case of hydrophobic particles the organic shell corresponds to the dodecanethiol layer, in the case of hydrophilic particles to the dodecanethiol layer plus the amphiphilic polymer around it.

The obtained core diameters of both samples are not the same, the polymer-coated particles have a slightly smaller core diameter ($<d>_{TEM}$ = 3.9 nm) than the hydrophobic ones ($<d>_{TEM}$ = 4.6 nm, see also Table SI-I.2 and Figure SI-I.3) although both were prepared from the very same batch of particles. This is due to the fractionating of the sample by the size exclusion column: After the polymer coating, only the center fractions eluted from the column were pooled to yield the final sample. Both front and tail shoulders containing larger or smaller particles were discarded, not necessarily yielding a symmetrically sharper size-distribution.

The effective diameters of the particles before and after polymer coating (which correspond to the particle Au core plus the organic layer around it) are derived from the first peak in the distance distribution function. In the case of the hydrophobic Au particles the effective particle diameter $<d_{eff}>_{TEM}$ has been determined to be 5.6 nm, whereby the diameter of the Au cores $<d>_{TEM}$ was 4.6 nm. . In the case of the hydrophobic Au particles the effective particle diameter has been determined to be 8.6 nm, whereby the diameter of the Au cores was 3.9 nm. As in the case of the semiconductor particles the thickness of the organic layer was calculated as ($<d_{eff}>_{TEM}$ -$<d>_{TEM}$)/2, the numeric values are shown in Table SI-II.2. The thickness of the dodecane thiol layer of the Au particles differs from the TOPO / HDA layer of the CdSe/ZnS or CdTe nanoparticles[5].

---

[5] From the length of the molecule, one would expect a thicker layer for dodecanethiol than for TOPO. However, also steric effects of the organic molecules might play a role: Dodecanethiol consists of one linear C12 (dodecyl) chain while TOPO has three C8 (octyl) chains. The latter might be more densely packed while the longer chains could allow an intercalation of the organic molecules which would lead to a smaller distance between the particles, especially in the dry state when prepared on the TEM grid. However, the differences are also within the error bars of our method.
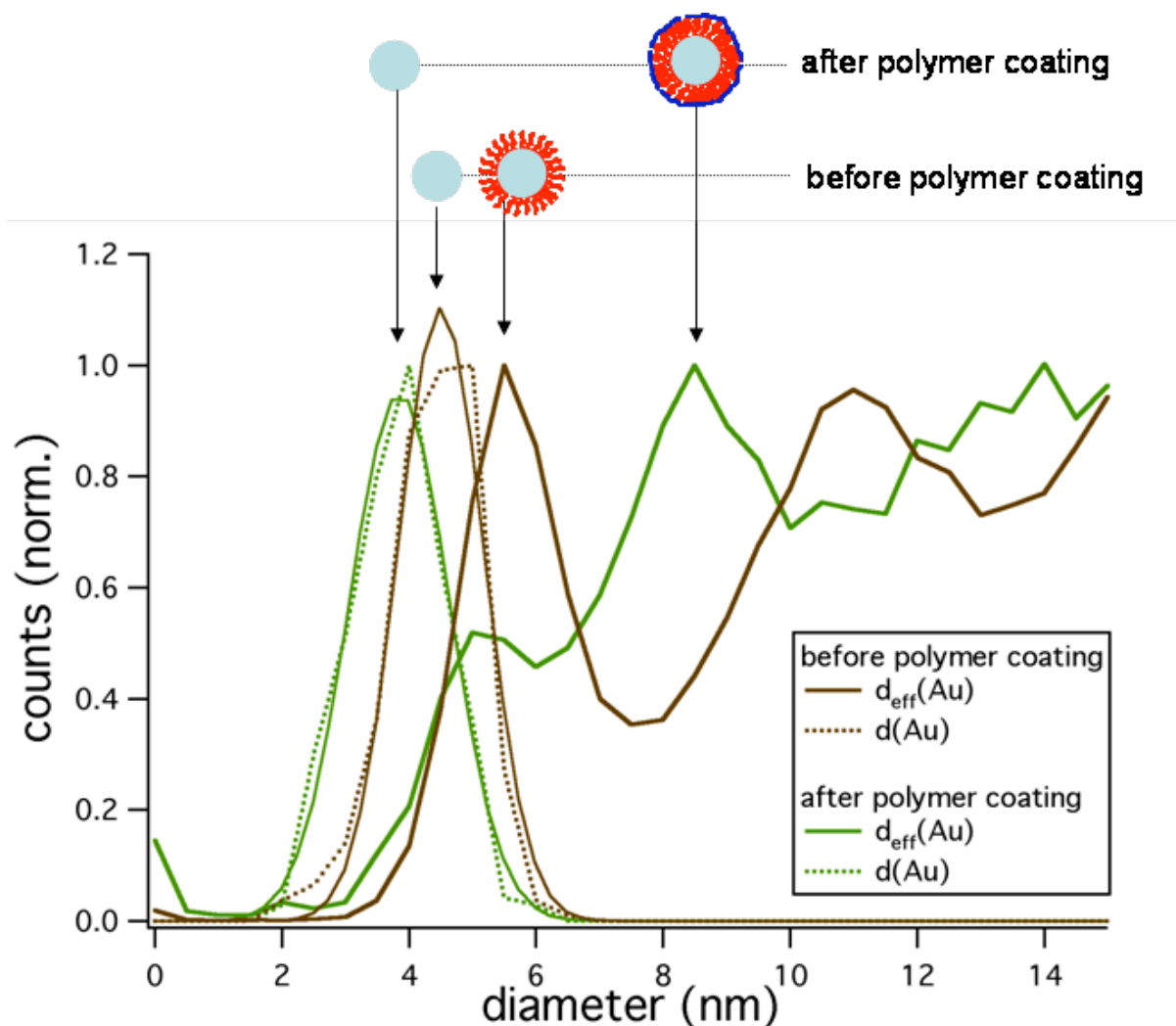
Figure SI-II.4: *Histograms of the core diameters <d> (solid lines) of Au nanoparticles capped with dodecanethiol (green) and coated with the amphiphilic polymer (brown) as obtained by TEM analysis. The graph also contains the distribution of the distances between the centers of the particles (dashed lines) for hydrophobic (green) and hydrophilic particles (brown), see Chapter II.1. The first peak in this distribution function can be interpreted as lower limit for the effective particle diameter $<d_{eff}>_{TEM}$, i.e. the diameter of the inorganic Au core plus the organic shell around the particle. In the case of hydrophobic particles the organic shell corresponds to the dodecanethiol layer ($<d_{eff}>_{TEM} = 5.6$ nm), in the case of hydrophilic particles to the dodecanethiol layer plus the amphiphilic polymer around it ($<d_{eff}>_{TEM} = 8.6$ nm).*
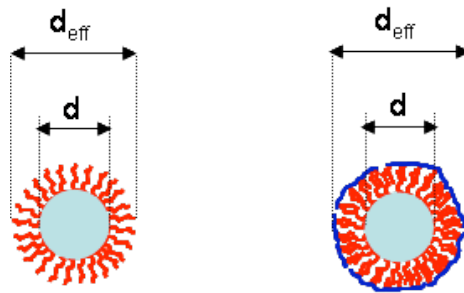
particle	thickness of the organic layer ($(\langle d_{eff}\rangle_{TEM} - \langle d\rangle_{TEM})/2$) before polymer coating	thickness of the organic layer ($(\langle d_{eff}\rangle_{TEM} - \langle d\rangle_{TEM})/2$) after polymer coating
CdTe	1.2 nm	2.8 nm
Au	0.5 nm	2.4 nm

Table SI-II.2: Thickness of the organic layer around the particles. $\langle d\rangle_{TEM}$ is the mean diameter of the inorganic cores as determined from the histograms of the diameter distribution from the TEM images. The effective particle diameters $\langle d_{eff}\rangle_{TEM}$ were obtained as the mean distance between the centers of adjacent particles. The effective diameters comprise the inorganic core of the particles plus the organic layer adsorbed to it. Before the polymer-coating the organic layer around the (hydrophobic) particles is TOPO/HDA and dodecanethiol in the cases of CdTe and Au particles. After the polymer-coating an additional layer of amphiphilic polymer adds to the organic layer of the (hydrophilic) particles. Again, the linear dodecanethiol molecules could allow a deeper intercalation with both the dodecanethiol capping of adjacent particles and the hydrophobic side-chains of the polymer, which could explain the smaller values for the thickness of the organic layer before and after the polymer coating in case of the Au particles.

III) Gelelectrophoresis experiments

Agarose gels of different w/v percentage were prepared with Agarose UltraPure (Invitrogen #15510027) and 0.5 x TBE buffer (Sigma-Aldrich, # T3913). For a typical 1% and 2 % gel, 1.5 g and 3 g of agarose were added to 150 ml 0.5 x TBE buffer in an Erlenmeyer flask, respectively, covered by a Petry dish and heated in a microwave oven. The heating was interrupted several times to shake the flask before boiling, so that the agarose could hydrate and finally form a homogeneous clear solution without sticking to the bottom of the flask. The agarose was left for about a minute in the microwave oven and was cast still hot into the gel tray mounted in the gel caster (Biorad Sub-Cell GT), before a comb for the wells was inserted. After the gels had become solid, the comb was removed and the gel was placed into the electrophoresis device (Biorad, #170-4401 Sub-Cell GT electrophoresis cells, 15 x 10 cm tray) filled with 0.5 x TBE. The electrophoresis was performed at 100 V constant voltage, after 60 min or more the gel was taken out and a digital picture was taken (Biorad GelDoc 2000). The electric field strength was estimated to be 10 V/cm.

Due to their negative charge the polymer-coated nanoparticles used in this study migrate towards the positive electrode. As control 10 nm phosphine coated Au nanoparticles were run on the same gel [10].

For each particle the length of the migration length l was measured and normalized to the migration length l_{10nm} of the phosphine-coated 10 nm Au particles to yield the relative electrophoretic mobility m/m_{10nm} of the particle (see Figure SI-III.1):

$$m_y/m_{10nm,y} = l_y / l_{10nm,y} \tag{1}$$

y hereby refers to the gel percentage (1% or 2%). In previous work [10] we have obtained a calibration curve (2) which relates the relative mobilities $m_y/m_{10nm,y}$ to effective diameters d_{eff} [6]:

$$d_{eff} = -T \ln (m_y/m_{10nm,y} / A) + 6 \text{ nm} \tag{2}$$

with the parameters A = 1.049 and 1.12) and T = 85 and 37.7 for 1 % and 2 % agarose gels [10]. Examples of gels are shown in Figures SI-III.1 and SI-III.2 and the derived effective diameters are enlisted in Tables SI-III.1 and SI-III.2.

When a few PEG molecules are attached per particle discrete bands can be resolved which correspond to Au particles with no, one, two, three, etc. PEG molecules per particle. In accordance with previous results [8] the spacing between the discrete bands increases with the molecular weight for both Au and CdSe/ZnS particles. The effective size of particles modified with one PEG molecule with a high molecular weight is always smaller than the same particles modified with two PEG molecules with each half the molecular weight. This is plausible since the radius of a polymer coil does not scale linearly with its molecular weight, thus two small polymer coils add more to the effective radius of a nanoparticle than one polymer molecule of the double molecular weight.

---

[6] This calibration curve was obtained by running particle standards with a known size on gels of the the same percentage. Phosphine-coated Au particles of known size (core diameter 5, 10, 15, 20, ... nm) were used and their effective diameters were estimated as the core diameter + 1 nm for the phosphine layer. The relative mobility versus the effective particle diameter was fitted with a monoexponential fit function for each gel percentage.

Also the nanoparticles saturated with PEG are more retarded when modified with PEG of higher molecular weight. With a molecular weight ≥ 5000 g/mol, the saturated nanoparticles migrate towards the negative electrode, indicating a positive net charge of the conjugated particles. This has already been found in earlier experiments and is always reproducible, yet the origin of the positive charge is not clear. We mention again the hypothesis of ion binding [8,11] to the originally neutral PEG chains that have a similar structure to crown ethers when coiled.
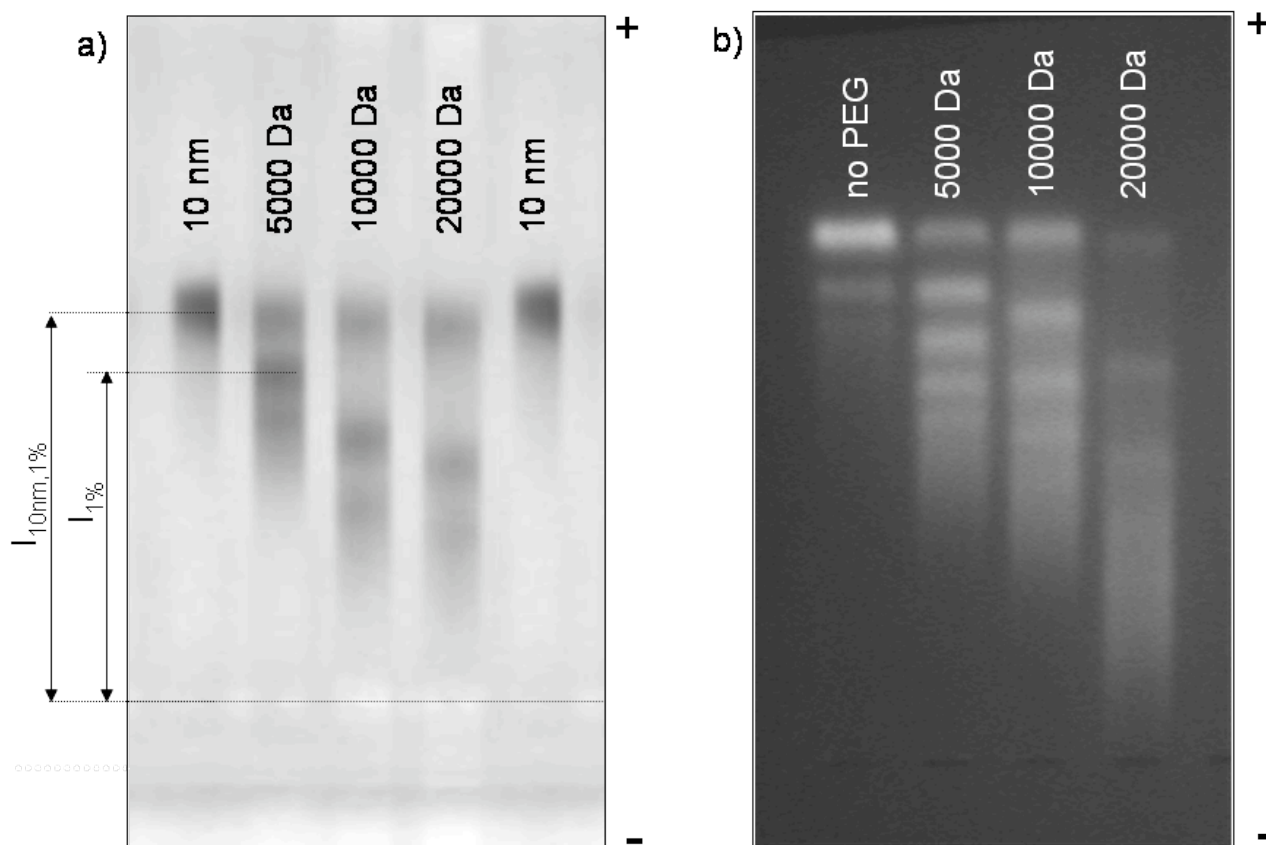

Figure SI-III.1: Polymer-coated Au (a) and CdSe/ZnS (b) nanoparticles to whose surface a small number of PEG molecules of different weight (5 kDa, 10 kDa, and 20 kDa) was attached were run for 1 @ 100 V on 1% agarose gels. The position of the bands on the gel was then recorded by taking a digital photograph of the gel. In the case of the fluorescent CdSe/ZnS particles the gel had been illuminated with an UV table during the photographing procedure. As the polymer coated particles are negatively charged the migrate towards the positive electrode. In the gel shown here with the Au particles (a) phosphine-coated Au particles of 10 nm Au-diameter were run as control on the gel [10]. In the case of the gel shown here for CdSe/ZnS particles plain polymer-coated CdSe/ZnS particles (i.e. without PEG) were run as control on the gel (b). For each band the length of migration $l_{1\%}$, i.e. the distance between the final position of the band on the gel and the position were the particles had been loaded into the gel, is measured. In order to obtain the relative mobility $m_{1\%}/m_{10nm,1\%}$ of the particles this length of migration is related to the length of migration of phosphine-coated Au particles of 10 nm Au diameter $l_{10nm,1\%}$ with Formula (1). Sometimes, as on the gel shown in (b) no 10 nm phosphine-coated Au-particles were run on the same gel. In this case an additional gel was run in which the mobility of the polymer-coated particles (without PEG) was related to the mobility of the 10 nm phosphine-coated Au-particles. More details about the evaluation of our gel electrophoresis experiments can be found in a previous report [10]. The discrete bands on the gel correspond to particles with no, one, two, etc. PEG molecules bound per particle [8].
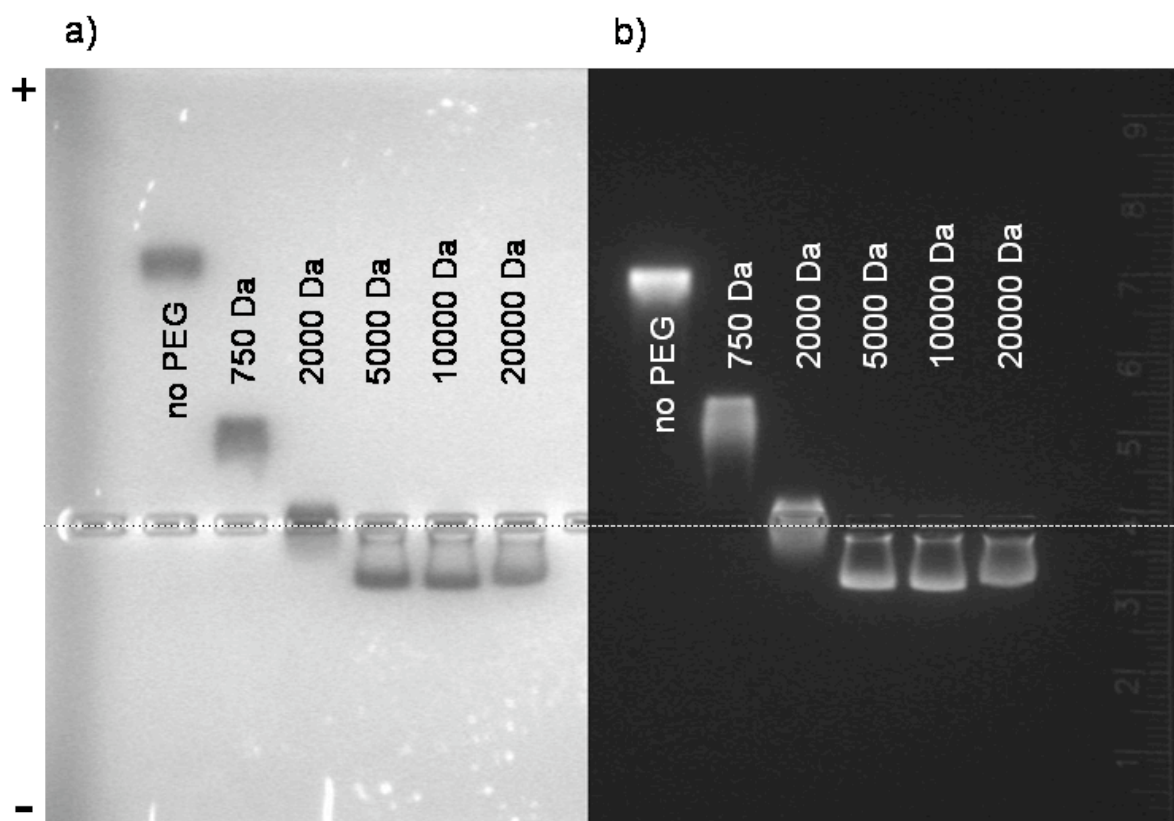
Figure SI-III.2: : *Polymer coated Au (a) and CdSe/ZnS (b) nanoparticles to whose was saturated with PEG molecules of different weight (0.75 kDa, 2kDa, 5 kDa, 10 kDa, and 20 kDa) were run for 1 @ 100 V on 2% agarose gels. The gels were photographed and the migration length of each band $l_{2\%}$ was measured and related to the migration length of phosphine-coated Au particles with 10 nm Au diameter (not shown on the gels presented here) in order to obtain relative mobilities with Formula (1). Upon saturation with PEG of molecular weight ≥ 5 kDa the particles migrate towards the negative electrode and therefore must posses an overall positive charge. The position where the particles had been loaded on the gel is marked with a dashed line.*

There are several restrictions on deriving effective diameters from relative mobilities with a calibration curve (2)[7] [10]. The particles used to obtain the calibration curve (2) were phosphine-coated Au nanoparticles and thus different in nature from the here used polymer-coated particles with attached PEG molecules. These particles were negatively charged and the particles of different diameter had the same charge density. However, for the particles used here upon attaching PEG not only the diameter but also the charge changes. Therefore, for the particles with a lot of PEG gel electrophoresis is not an adequate method to determine their effective diameter, since it is in this case evident that the changes in mobility are not only due to the particles' size but also due to their change in charge that even changes the sign. The calibration curve (2) can only be applied for particles which are similar in nature to phosphine-coated Au particles. For polymer-coated Au particles with only few PEG molecules attached per particle the charge effect upon binding PEG can be neglected and curve (2) can be applied. The values obtained with (2) for particles saturated with PEG of high molecular weight on the other hand have to be disregarded.

---

[7] The calibration curve is a fit to effective mobility of particles whose effective diameters are known or can be estimated. As it is a fit values derived from the fit do not necessarily match exactly the values which have been used to generate the fit.

PEG/ polymer-coated CdSe/ZnS particle	M(PEG) [g/mol]	$m_{1\%}/m_{10nm,1\%}$	$m_{2\%}/m_{10nm,2\%}$	$<d_{eff}>_{gel(1\%)}$ [nm]	$<d_{eff}>_{gel(2\%)}$ [nm]
0	5000	0.95	0.89	14.5	14.5
1	5000	0.84	0.79	24.5	19.3
2	5000	0.75	0.69	34.2	24.1
3	5000	0.67	0.62	43.6	28.5
4	5000	0.61	0.55	51.9	32.8
5	5000	-	0.50	-	36.7
6	5000	-	0.44	-	40.8
0	10000	0.95	-	14.5	-
1	10000	0.80	-	29.4	-
2	10000	0.67	-	43.5	-
3	10000	0.60	-	56.5	-
0	20000	0.95	-	14.5	-
1	20000	0.71	-	39.6	-
2	20000	0.54	-	62.7	-
0	-	-	0.89	-	14.5
sat.	750	-	0.39	-	46.1
sat.	2000	-	0.01	-	180.2
sat.	5000	-	-0.22	-	* neg.
sat.	10000	-	-0.22	-	* neg.
sat.	20000	-	-0.21	-	* neg.

Table SI-III.1: Relative mobilities $m_y/m_{10nm,y}$ and effective particle diameters $<d_{eff}>_{gel,y}$ for polymer-coated CdSe/ZnS particle with attached PEG molecules of different molecular weight. y codes the gel percentage (1% or 2%). In the upper columns particles with a discrete number of PEG molecules (0, 1, 2, ... PEGs per particle) are enlisted. In the lasts columns particles whose surface had been saturated with PEG are enlisted. The relative mobilities $m_y/m_{10nm,y}$ were derived by measuring the migration lengths l_y of the particles and normalizing them to the migration lengths $l_{10nm,y}$ of phosphine-coated Au particles of 10 nm Au diameter by using Formula (1). The effective diameters were derived from the relative mobilities by using a calibration curves (Formula (2)) which had been obtained previously [10]. In case of particles saturated with PEG of high molecular weight the mobilities became very small or even negative. Negative mobilities mean that the particles migrated towards the negative instead of the positive electrode. This comes due to a charge effect and in this case the calibration curve (2) can no longer be applied. The values labeled with (*) therefore have to be disregarded.

PEG/polymer-coated Au particle	M(PEG) [g/mol]	$m_{1\%}/m_{10nm,1\%}$	$m_{2\%}/m_{10nm,2\%}$	$<d_{eff}>_{gel(1\%)}$ [nm]	$<d_{eff}>_{gel(2\%)}$ [nm]
0	5000	0.97	0.94	12.7	12.5
1	5000	0.83	0.81	26.3	18.4
2	5000	0.72	0.69	38.2	24.5
3	5000	-	0.59	-	29.9
0	10000	0.96	0.94	13.4	12.5
1	10000	0.67	0.74	44.5	21.6
2	10000	0.49	0.60	70.7	29.3
0	20000	0.95	0.94	14.4	12.5
1	20000	0.61	0.63	52.5	27.7
2	20000	0.42	0.45	83.5	40.2
0	-	-	0.94	-	12.5
sat.	750	-	0.35	-	49.7
sat.	2000	-	0.03	-	140.1
sat.	5000	-	-0.20	-	* neg.
sat.	10000	-	-0.21	-	* neg.
sat.	20000	-	-0.20	-	* neg.

Table SI-III.2: Relative mobilities $m_y/m_{10nm,y}$ and effective particle diameters $<d_{eff}>_{gel,y}$ for polymer-coated Au particle with attached PEG molecules of different molecular weight. y codes the gel percentage (1% or 2%). In the upper columns particles with a discrete number of PEG molecules (0, 1, 2, ... PEGs per particle) are enlisted. In the lasts columns particles whose surface had been saturated with PEG are enlisted. The relative mobilities $m_y/m_{10nm,y}$ were derived by measuring the migration lengths l_y of the particles and normalizing them to the migration lengths $l_{10nm,y}$ of phosphine-coated Au particles of 10 nm Au diameter by using Formula (1). The effective diameters were derived from the relative mobilities by using a calibration curves (Formula (2)) which had been obtained previously [10]. In case of particles saturated with PEG of high molecular weight the mobilities became very small or even negative. Negative mobilities mean that the particles migrated towards the negative instead of the positive electrode. This comes due to a charge effect and in this case the calibration curve (2) can no longer be applied. The values labeled with (*) therefore have to be disregarded.

If one analysis the band of polymer-coated CdSe/ZnS particles in Figure SI-III.1b carefully one can observe three bands, whereby the fastest one corresponds to single polymer-coated CdSe/ZnS particles. As there was no PEG linked to these particles one would not expect the two additional bands. Their corresponding diameters (1% gel, diameters derived with (2) from the relative mobilities) are enlisted in Table SI-III.3. As these particles never have been in contact with any PEG they can be explained in two ways: first, two or three particles might be embedded in the same polymer shell, and second, two or three polymer-coated particles might stick nonspecifically together. We cannot decide which of the two possibilities is true. We have to point out that the same effect (3 bands) is true for the commercially available polymer-coated CdSe/ZnS particles from the Quantum Dot Corp. However, if one compares the intensities of the bands it is obvious, that the fraction of particles in the 2nd and 3rd band is very small compared to the 1st band with the single polymer-coated particles. The 2nd and 3rd band only can be observed in the case of CdSe/ZnS, as these bands are much sharper, but not in the case of Au, where the bands cannot be resolved as well (see Figure III.3.1). Therefore these impurities can be neglected. It is also important to point out that these impurities have nothing to do with

the bands generated by the attachment of PEG. The higher the molecular weight of single PEG molecules attached to the particles, the bigger their shift on the gel becomes. Therefore, the discrete bands in the case of attachment of single PEG molecules are a specific effect with high yield and must not be confused with the small impurities in the plain particle samples. This effect has also been observed with commercial (plain polymer-coated) nanoparticles (QuantumDots QD655 ITK carboxyl, data not shown).

band #	$d_{eff,1\%}$ [nm]
1	14.5
2	23.7
3	30.2

Table SI-III.3: Effective diameters corresponding to the bands resolved with plain polymer-coated CdSe/ZnS particles on a 1% agarose gel by using Formula (2). The first band corresponds to the actual single polymer-coated CdSe/ZnS particles, whereas the two slower bands are impurities. The first band corresponds to the data shown in Table SI-III.1 for CdSe/ZnS particles with no PEG attached per particle.

IV) Size exclusion chromatography (SEC) experiments

The setup consisted of an Agilent 1100 HPLC system, comprising a vacuum degasser (G1322A), a quaternary pump (G1311A), an autosampler (G1313A ALS) with 900 ul injection upgrade kit (G1363A) and multidraw upgrade kit (G1313-68711), a column oven with column switching valve (G1316A), a diode array detector DAD (G1365B with upgrade G1315), a FLD (G1321A) and a fraction collector (G1364A), operated with the Chemstation B.01.03 software. All components before the column were connected by stainless steel or PEEK capillaries of an inner diameter (ID) of 0.17 - 0.3 mm, and after the column of ID 0.5 mm in order to reduce the back pressure at the column.

The mobile phase for all experiments was 50 mM sodium borate buffer with 100 mM NaCl, pH 9.0 ("SBBS") at a flow rate of 0.5 ml/min. The elution was observed with the DAD by measuring the absorption simultaneously at different wavelengths in the UV and visible range, optionally also the fluorescence. All experiments were performed with the column at room temperature. As stationary phase, different polymer-based gels (GE Healtcare Sephacryl S-300, S-400, S-500 and S-1000 and Tosoh Toyopearl HW75-F and HW65-S) were packed into empty columns (GE Healthcare XK16-70 or Omnifit ID x L = 15 x 750 mm) according to the instructions of the manufacturer. The column dimensions were chosen so that the columns could also be used for injection volumes of 1 ml per run for preparative purposes. Glass columns were preferred because they have the advantage of easy visual control of the gel bed in case of gaps, cracks, air or other contamination.

For the column calibration, first the void volume v_0 and the total liquid column volume v_t, that is accessible for small molecules and the mobile phase, were determined with λ-DNA and 3 % acetone, respectively. λ-DNA consists of 48.5 kbp, has a molecular weight of $31.5 \cdot 10^6$ g/mol and a gyration radius in the order of 600 nm, which is still small compared to the particle size of the stationary phase (47 μm for the Sephacryl media). The λ-DNA was assumed to be totally excluded from the gel pores since it eluted always earlier than the often used blue dextran (M_W $2 \cdot 10^6$ g/mol, e.g. Sigma-Aldrich # D5751), and yielded a much more symmetric peak. That means for the column materials used in these experiments, that the blue dextran could enter the pores of the gel beads at least partially and is therefore not a good standard. To prepare the standard sample solution for the determination of v_0 and v_t, 40 μl of a λ-DNA stock (Fermentas #SD0021, as received) and 30 μl of acetone were added to 930 μl SBBS and mixed well with a pipette prior to injection.

A slight dependence of the flow rate and injection volume on the elution volume v_e was observed. Therefore the flow rate was set to 0.5 ml/min and the injection volume to 200 μl for all measurements that have been performed in this study. In order to compare the resolution of different packing materials in different columns, the distribution coefficient K_{SEC} was calculated from the elution volume v_e at the peak maxima with the total liquid volume v_t and the void volume v_0

$$K_{SEC} = (v_e - v_0)/(v_t - v_0)$$
$$= (t_e - t_0) / (t_t - t_0) \tag{1}$$

Formula (1) can also be written in the same way by using elution times t instead of elution volumes. When the retardation of a sample is due to size exclusion only (without any attractive forces between the eluent and stationary phase), the partition coefficient K_{SEC} is found by principle between 0 and 1 and equals to the fraction of the pore volume $(v_t - v_0)$ of the

stationary phase that is accessible for the molecule or particle of interest. By referring to the partition coefficient K_{SEC}, differences in the dimensions or filling of different columns is cancelled out and the resolution range of the different materials can be directly compared. Thus K_{SEC} in first order does not depend on the actually used columns, but only on the different gels with which the columns are filled with.

In Figure SI-IV.1, the partition coefficients K_{SEC} for a number of samples run on size-exclusion columns with different polymer-based materials are shown. The column materials were chosen because they have relative large pores which are needed to resolve nanoparticles of different size, and they are stable at basic pH (in contrast to silica-based materials) where the polymer-coated nanoparticles are most stable. The column dimensions inner diameter times length (ID x L) of 16 mm x 700 mm (GE Healthcare XK16/70) and 15 mm x 750 mm (Omnifit) were chosen because they also allow for small-scale preparative runs with an injection volume of 1 ml/run. Running two columns in series would only improve the total separation in regard of elution time or volume, and eventually the separation of discrete peaks, but the relative separation in terms of K_{SEC} would be the same.
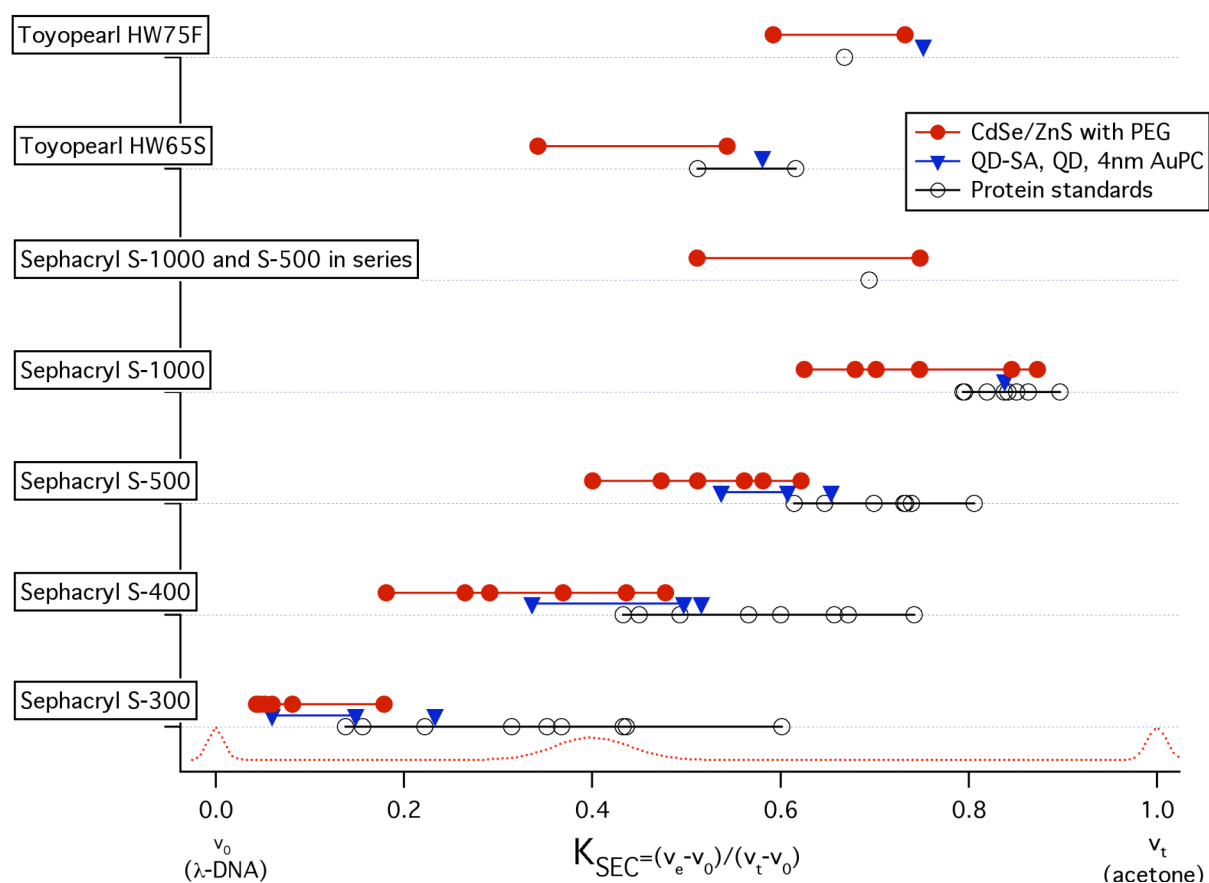

Figure SI-IV.1: Partition coefficients K_{SEC} of different standard samples and particles measured on different columns. The partition coefficient of different protein standards are plotted as black circles. The partition coefficients of CdSe/ZnS samples which are saturated with PEG molecules of different molecular weight are plotted as red circles. The partition coefficients of Au samples and commercially available quantum dot samples are plotted as blue triangles. For the purpose of size-determination of nanoparticles the column material is best suited, which offers the best overlap of the range of partition coefficients spanned by the protein standards with the range needed for the nanoparticles. All values are enlisted in Table SI-IV.1.

sample name	Sephacryl S-300	Sephacryl S-400	Sephacryl S-500	Sephacryl S-1000	Sephacryl S-1000 + Sephacryl S-500	Toyopearl HW65S	Toyopearl HW75F
Thyroglobulin bovine	0.156	0.450	0.615	0.820	0.694	0.512	0.668
Thyroglobulin porcine	0.138	0.433	0.615		-	-	-
Apoferritin	0.222	0.493	0.647	0.796	-	-	-
Beta-Amylase	0.315	0.566	0.699	0.837	-	-	-
Alcohol Dehydrogenase	0.367	0.600	0.739	0.863	-	-	-
Albumin	0.433	0.657	0.731	0.842	-	-	-
HSA	0.436	0.672	-		-	0.616	-
Carbonic Anhydrase	0.601	0.742	0.806	0.897	-	-	-
CdSe/ZnS	0.179	0.478	0.622	0.873	0.749	0.543	0.718
CdSe/ZnS + M_W 750 PEG	0.060	0.436	0.581	0.846	-	-	-
CdSe/ZnS + M_W 2000 PEG	0.082	0.369	0.562	0.748	-	-	-
CdSe/ZnS + M_W 5000 PEG	0.053	0.291	0.512	0.702	-	-	-
CdSe/ZnS + M_W 10000 PEG	0.047	0.265	0.473	0.680	-	-	-
CdSe/ZnS + M_W 20000 PEG	0.043	0.181	0.400	0.625	0.511	0.616	0.570
Au	0.233	0.516	0.653	0.838	-	0.581	0.738
QD655 carboxyl	0.149	0.497	0.607	-	-	-	-
QD655 SA	0.060	0.336	0.537	-	-	-	-

Table SI-IV.1: Partition coefficients of different standard samples and particles measured on different columns. In the first column the names of the different samples are given. The first nine samples are different protein standards (see Table SI-IV.2 for more information). The next 6 samples are the polymer-coated CdSe/ZnS samples used for this study (see Chapter I.1, I.4, and I.6). The surface of these particles is saturated with PEG molecules of different molecular weights (no PEG, 750, 2000, 5000, 10000, 20000 g/mol). The next sample is polymer-coated Au used for this study: 4 nm polymer-coated Au particles (see Chapter I.3, I.4). The two last samples are commercial quantum dots (Quantum Dot Corp., Hayward, CA, USA: CdSe/ZnS with polymer shell fluorescent at 655 nm with carboxyl-, and streptavidin- (SA) modification). The data are graphically displayed in Figure SI-IV.1.

The results of Figure SI-IV.1 demonstrate that different column materials resolve particles of different size. This can be seen very nicely in the "family" of Sephacryl gels, which from S-300 to S-1000 have pores with increasing size. For the gel with the biggest pores (Sephadex S-1000) the protein standards elute at very high partition coefficients (close to the limit $K_{SEC} = 1$ ultimately small molecules). For the gels with smaller pores the protein standards are eluted at much lower elution times and they also span from the smallest to the biggest protein a larger range in the interval $0 \leq K_{SEC} \leq 1$. The standard protein samples shown in Figure SI-IV.1 therefore certainly can be best resolved by size with the Sephadex S-300 gel. As it becomes also obvious from the data of Figure SI-IV.1 the nanoparticles samples used in this study are

significantly bigger than the protein standards. Therefore they are eluted at smaller partition coefficients. This already points out a severe limitation of size measurements of nanoparticles with size exclusion columns: There are no appropriate size-standards easily available. The nanoparticles are best resolved with the gel with the biggest pores (biggest interval in K_{SEC} for Sephacryl S-1000), but for this gel the protein standards are not resolved well, as they are too small. When comparing the interval of K_{SEC} values that is spanned by the series of protein standards or nanoparticle samples, the Sephacryl S-400 material shows the best performance for both protein standards and nanoparticle samples. Thus in the following, the evaluation is focused on this material and the Sephacryl S-300 and S-500 with smaller or larger pores, respectively.

For size determination by size exclusion chromatography, columns have to be calibrated with standards of known molecular weight and/or radius, and from the elution time, volume or K_{SEC} value of a sample its size can be derived. For SEC with aqueous mobile phases several types of standards exist like synthetic polymers and proteins [12], also nanoparticles have already been used for column characterization [13]. Actually, the elution volume of a sample does not directly depend on the molecular weight, but on its hydrodynamic volume. The hydrodynamic volume naturally depends on the molecular weight of a given molecule, but the M_W-volume relation might depend on the kind of molecule. By taking into account the hydrodynamic volume (or hydrodynamic radius r_h by assuming spherical molecules) instead of M_W, different standards can be used for a so-called universal calibration [14].

Globuar proteins have a compact shape and can be approximated as spheres with a hydrodynamic radius r_h (in nm) dependent of the molecular weight M_W (in g/mol) by the following expression [15,16]:

$$r_h = 0.081 \, M_W^{1/3} \tag{2}$$

Name of the molecule	#	M_W (g/mol)	r_h (nm)	K_{SEC} S-300	K_{SEC} S-400	K_{SEC} S-500
λ-DNA (48502 base pairs)	v_0	31500000	≥ 500	0	0	0
Thyroglobulin bovine (MWGF1000)	1a	669000	7.084	0.156	0.450	0.615
Thyroglobulin porcine (#89387)	1b	669000	7.084	0.138	0.433	0.615
Apoferritin (MWGF1000)	2	443000	6.175	0.222	0.493	0.647
Beta-Amylase (MWGF1000)	4	200000	4.737	0.315	0.566	0.699
Alcohol Dehydrogenase (MWGF1000)	5	150000	4.304	0.367	0.600	0.739
Albumin (MWGF1000)	6	66000	3.273	0.433	0.657	0.731
HSA (A3782)	7	60000	3.171	0.436	0.672	-
Carbonic Anhydrase (MWGF1000)	8	29000	2.489	0.601	0.742	0.806
acetone	v_t	58	< 0.5	1	1	1

Table SI-IV.2: _Molecular weights and estimated hydrodynamic radii (derived with Formula (2) of several protein standards, and their K_{SEC} values for three different Sephacryl columns. The numbers in parentheses indicate the product number from Sigma-Aldrich. λ-DNA and acetone are used as limit for big and small molecules, respectively. The K_{SEC} values for the Sephacryl S-400 gel have been derived from the measurements shown in Figure SI-IV.2._

In Table SI-IV.2 a number of proteins with radii derived by their molecular weight according to Formula (2) are enlisted. It has to be noted that for globular proteins, other radii than the ones derived with Formula (2) have been reported in literature [17], and even if the protein structure is

known, sizes obtained from protein crystals (e.g. from the RCSB Protein Data Bank) are naturally not the same for hydrated proteins in solution

For each of the protein standards the partition coefficient was determined for different gels. In Figure SI-IV.2 the measurements for the Sephacryl S-400 filled column are shown. The partitions coefficients derived from this measurement according to Formula (1) and also the ones obtained with other gels are enlisted in Table SI-IV.1.
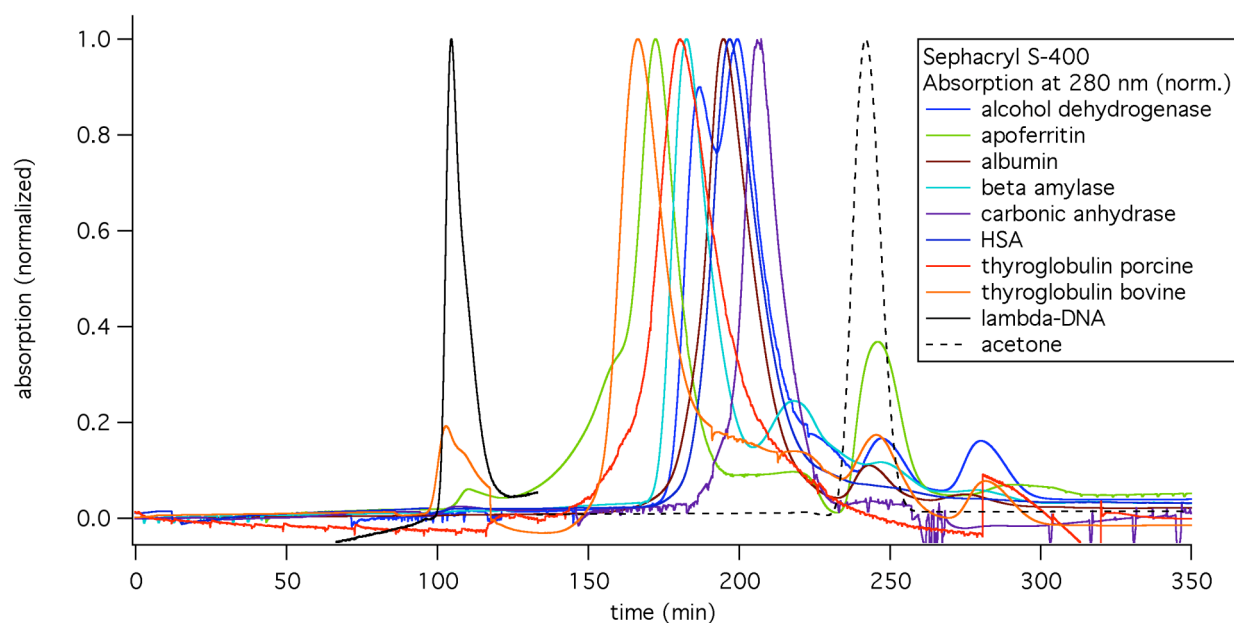

Figure SI-IV.2: Chromatograms of protein standards. The normalized absorption at 280 nm of the elute solution is plotted versus the elution time. Larger proteins elute first. The elution times of the peak maxima were used to calculate the K_{SEC} values shown in Table SI-IV.2. Lambda-DNA and acetone were injected in the same run, for clarity the peaks are normalized separately for this graph.

The elution time, volume or respectively K_{SEC}, now can be related to the hydrodynamic radius according to Table SI-IV.2 (and Formula (2) which leads to a calibration curve that relates partition coefficients K_{SEC} to hydrodynamic radii r_h, see Figure SI-IV.3. An empirical finding for globular proteins is that in a certain range for a size-exclusion column there is a linear dependence between the logarithm of the molecular weight and the elution time, volume or partition coefficient K_{SEC}. According to Formula (2) this also yields to a linear relation between the logarithm of the hydrodynamic radius r_h and the partition coefficient K_{SEC}:

$$\log r_h = a \cdot K_{SEC} + b \qquad\qquad (3)$$

It is obvious that Formula (3) can only be valid for an intermediate range $0 \ll K_{SEC} \ll 1$. K_{SEC} = 0 refers to the exclusion volume and therefore to the M_W or radius of the standard sample (here λ-DNA) with a molecular weight of at least one order of magnitude bigger compared to the samples of interest. However, K_{SEC} would be also = 0 for any molecule bigger than λ-DNA. The case K_{SEC} = 1 (here determined with acetone) refers to ideally small molecules, with a M_W or radius close to 0. However, K_{SEC} would be also = 1 for any molecule smaller than acetone. Therefore the linear relation between $\log r_h$ and K_{SEC} is not valid for K_{SEC} close to 1 or close to 0. Also various other models and functions have been used to describe the relation between r_h and K_{SEC} alternative to Formula (3) [15]. Formula (3) has rather to be seen as an empirical instead of an analytical function. In addition, the exact shape of the $r_h(K_{SEC})$ calibration curve also

depends on parameters that are not at all included in the model, e.g. the shape and size distribution of the pores of the stationary phase, or any possible non-ideal behavior like electrostatic or hydrophobic interactions between the sample and the column.

The K_{SEC} data shown in Table SI-IV.2 for different protein standards with known r_h were fitted with Equation (3) with the fit parameters A and B. The fits are shown for three different column materials in Figure SI-IV.3 and the resultant fit parameters are summarized in Table SI-IV.3. By inverting Equation (3) now any measured K_{SEC} value can be converted in a corresponding hydrodynamic radius r_h:

$$r_h(K_{SEC}) = A \exp(-B \, K_{SEC}) \tag{4}$$

Expression (4) was then used in the following to convert the K_{SEC} values obtained for nanoparticles into hydrodynamic radii.

Effective diameters are assumed as two times the hydrodynamic radius:
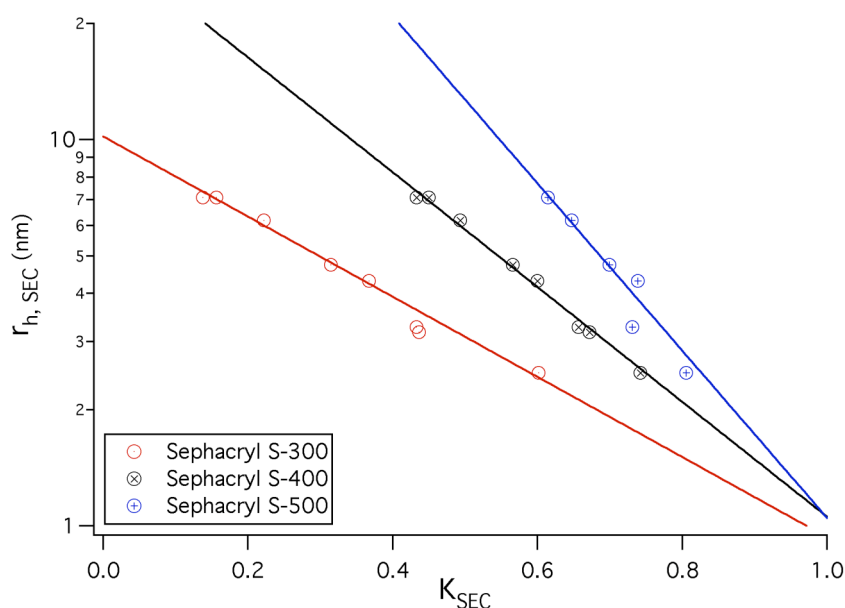
$$d_{eff} = 2 \cdot r_h \tag{5}$$

Figure SI-IV.3: K_{SEC} *values obtained from protein standards for different column materials. The hydrodynamic radii of the proteins r_h are plotted as derived from Equation (2) (numerical values as in Table SI-IV.2). A mono-exponential function $r_H = A \exp(-B \, K_{SEC})$ has been fitted to the data points with the fit parameters A and B. The resulting fit parameters are enlisted in Table SI-IV.3.*

Column material	Fit parameter A	Fit parameter B	range of K_{SEC} for used proteins
Sephacryl S-300	10.2 ± 1.3	2.39 ± 0.47	0.14 – 0.60
Sephacryl S-400	32.4 ± 5.7	3.42 ± 0.34	0.43 – 0.74
Sephacryl S-500	154 ± 166	4.99 ± 1.62	0.62 – 0.81

Table SI-IV.3: Parameters A and B of Function (3) which can be used to relate partition coefficients K_{SEC} with hydrodynamic radii r_h. A and B have been determined from the data shown in Figure SI-IV.3.

All the protein standards are eluted in different K_{SEC} ranges (Table SI-IV.3) as expected for the three Sephacryl materials with their three different pore sizes. The nanoparticle samples elute always before or around the biggest protein standard (thyroglobulin), so that the fit function has to be extrapolated in order to derive their hydrodynamic radii. In case of the column material with the smallest pores (Sephacryl S-300), the protein standards fit best to the well-resolved range, while the nanoparticle samples are "squeezed" close to the void volume v_0, or respectively $K_{SEC} = 0$. The assumed linear dependence holds not for K_{SEC} values close to 0 where the real slope has to become much steeper towards 0, so the simple exponential fit (3) delivers too small radii for any K_{SEC} value close to 0. In case of the column material with large pores (Sephacryl S-500), the proteins standards are "squeezed" into a range of K_{SEC} close to 1. Because the fit of the exponential function is now based on a very small range $K_{SEC} = 0.62$ - 0.81, the extrapolation to smaller K_{SEC} values cannot be reliable. The resolution of the column material Sephacryl S-400 is relatively good for both, the protein standards and nanoparticle samples, therefore it was chosen as the gel to be used best for the size characterization. For preparative purposes the situation can be different: E.g. for the separation of polymer-coated nanoparticles from unbound polymer (micelles), the Sephacryl S-300 shows a better performance.

As nanoparticle samples, the series of Au and CdSe/ZnS particles saturated with PEG of different molecular weight described above was run on the size exclusion columns. Figures SI-IV.4 and SI-IV.5 show as an example the chromatograms of CdSe/ZnS nanoparticles (absorption measured at 280 nm, due to the better signal-to-noise ratio compared to the wavelength of their exciton peak) and of Au nanopartcivles (absorption measured at 515 nm) and) run on a Sephacryl S-400 column. Similar to the protein standards, the elution times (peak maxima) were converted to K_{SEC} values (Tables SI-IV.1 and SI-IV.4.). From the K_{SEC} values then the hydrodynamic radii r_h were calculated by the inverse fit function (4) together with the fit parameters A and B (Table SI-IV.3) that were obtained from the protein standards. The hydrodynamic radii are enlisted in Table SI-IV.4.
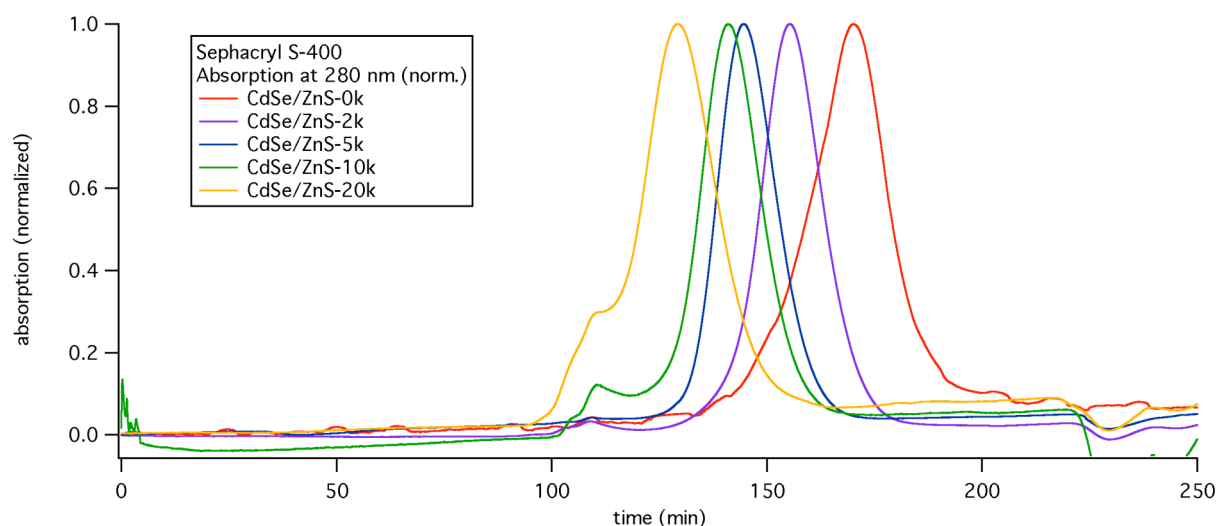

Figure SI-IV.4: *Chromatograms of CdSe/ZnS nanoparticles saturated with PEG of different molecular weight.*
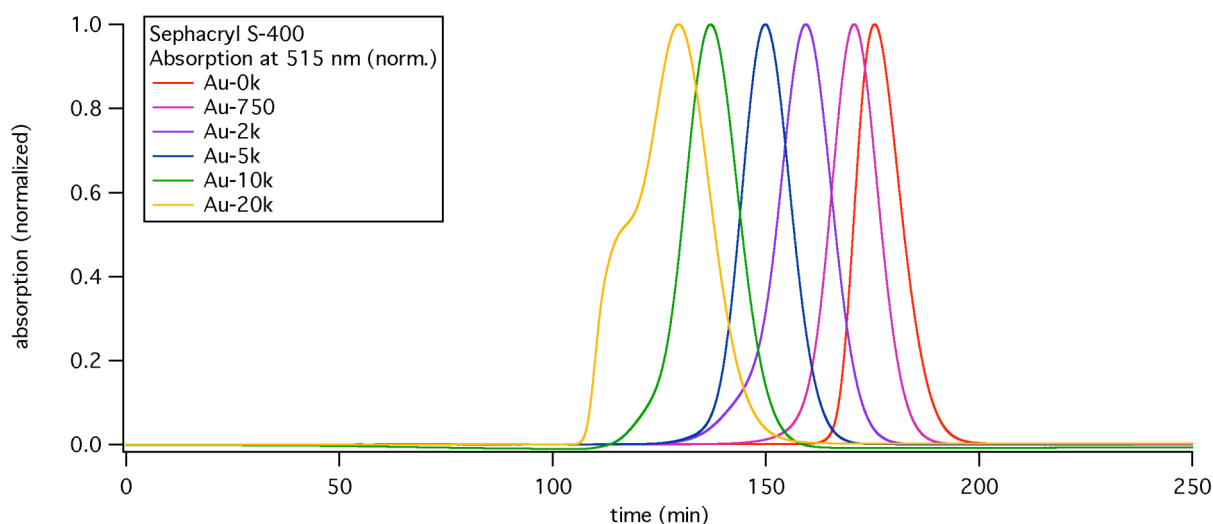
Figure SI-IV.5: Chromatograms of Au nanoparticles saturated with PEG of different molecular weight.

In Figure SI-IV.6, the calculated radii for Au and CdSe/ZnS particles with polymer-coating and PEG of different molecular weight are plotted. In contrast to Figure SI-IV.3 the scale for the hydrodynamic radius r_h is now linear, and also the 95 % expectation interval (internal functions of Igor software (Wavemetrics, V5.05)) is plotted. Based on the expectation interval, an error of about ± 2 nm in the determined size can be estimated for the larger PEG-modified nanoparticles in the case of the column packed with Sephacryl S-400.
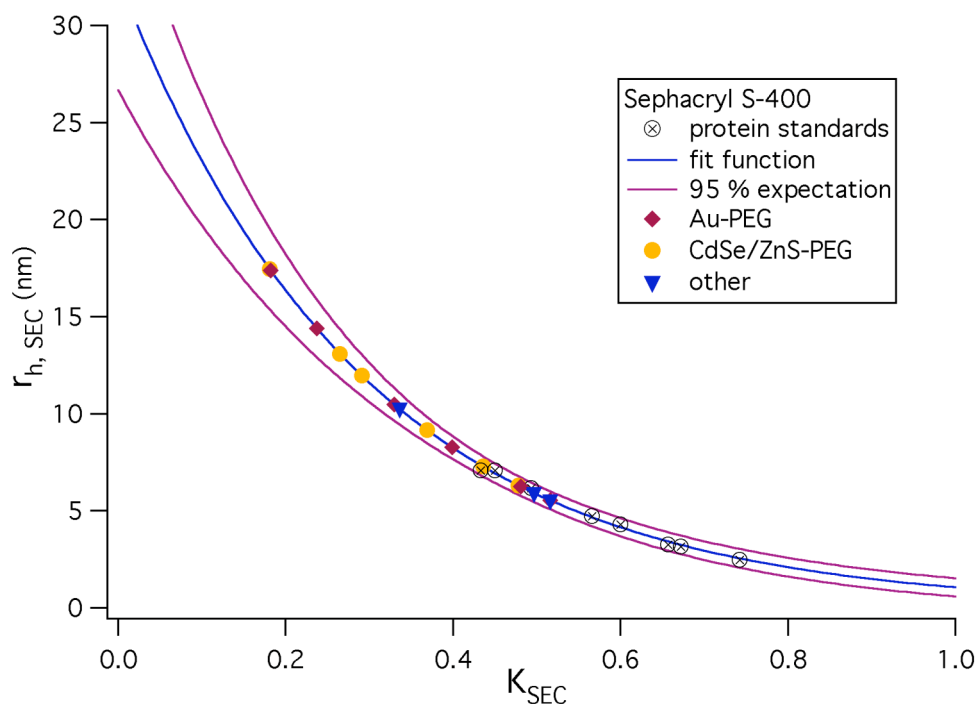

Figure SI-IV.6: The protein standards with the fitted and extrapolated exponential function (4) are shown here with a linear scale, together with the 95 % expectation interval. The radii of the nanoparticle samples were calculated from their K_{SEC} value with the same fit function. The numeric values are given in table SI-IV.4. This Figure demonstrates the error in the derived hydrodynamic radii due to deviations in the parameters A and B in the fit function.

Particles	Mw(PEG)	S-300 K_{SEC}	S-300 r_h (nm)	S-400 K_{SEC}	S-400 r_h (nm)	S-500 K_{SEC}	S-500 r_h (nm)
CdSe/ZnS	0	0.179	6.65	0.478	6.31	0.622	6.91
CdSe/ZnS	750	0.082	8.39	0.436	7.29	0.581	8.44
CdSe/ZnS	2000	0.060	8.84	0.369	9.17	0.562	9.32
CdSe/ZnS	5000	0.053	9.00	0.291	11.97	0.512	11.93
CdSe/ZnS	10000	0.047	9.12	0.265	13.08	0.473	14.48
CdSe/ZnS	20000	0.043	9.20	0.181	17.44	0.400	20.83
Au	0	0.233	5.85	0.516	5.54	0.653	5.89
Au	750	0.172	6.76	0.481	6.25	0.629	6.67
Au	2000	0.113	7.78	0.399	8.27	0.579	8.53
Au	5000	0.055	8.93	0.330	10.47	0.546	10.07
Au	10000	0.042	9.23	0.237	14.40	0.456	15.76
Au	20000	0.039	9.28	0.182	17.38	0.407	20.11
QD655 carboxyl		0.149	7.15	0.497	5.91	0.607	7.41
QD655 SA		0.060	8.84	0.336	10.26	0.537	10.54

Table SI-IV.4: *Nanoparticles run on Sephacryl S-300, S-400, and S-500 columns. Enlisted are the K_{SEC} values and the hydrodynamic radii r_h derived by fit function (4) with the parameters from Table SI-IV.3.*

For the size calibration, the series of globular proteins were run on the columns and the peak position was recorded at the maxium at 280 nm, where proteins as well as lambda-DNA and acetone absorb light. Protein solutions were prepared at a concentration of 2 – 10 mg/ml in either SBBS or 1 x protein stabilizing cocktail (Pierce #89806). Alcohol dehydrogenase eluted later after longer storage, so the solution was always prepared freshly prior to injection. Catalase (from bovine liver, Sigma-Aldrich #C1345) yielded a slightly turbid solution and precipitated over time. Since also the K_{SEC} values were larger than expected from the molecular weight and did not fit to the calibration curve, the data was not taken into account.

It has to be noted that the particle radii are derived from a function extrapolated from the data points of the protein standards. It would be desirable to have larger particle standards available in order to be able to have a truly *interpolated* calibration curve also for radii between e.g. 10 and 20 nm. For the column calibration, also commercial Au particles (British Biocell) of diameters between 5 and 15 nm were tried, with different surface modifications: the particles were coated with phosphine (bis(p-sulfonatophenyl)phenylphosphine dihydrate dipotassium salt, Strem Chemicals #15-0463), and MPA (mercaptopropionic acid, Sigma-Aldrich # M5081) by incubating the Au particle solution with some mg phosphine or MPA for several days, so that the citrate shell was replaced. An empty disposable plastic syringe was packed with some Sephacryl medium after the outlet had been stuffed with some glass wool, and equilibrated with SBB or SBBS driven by gravity. However, even in the case of SBB, 5 nm particles coated with MPA or phosphine got stuck in the stationary phase and were visible as a bluish band. For both cases, no free MPA or phosphine had been added to the mobile phase. Also 55 nm blue latex beads (Sigma-Aldrich #L1148) did not pass the small test column. In lack of a refractive index detector, plain PEG standards could not be measured since it shows no optical absorption or fluorescence in the wavelength range 200 – 800 nm.

There are already a number of publications about SEC with colloidal nanoparticles in both aqueous [18-22] or organic solvents [23-25], however in most cases either surfactants or precursors for the core material were added to the mobile phase in order to insure the stability of the colloids. For a reliable comparison, both size standards and samples should be run in the same mobile phase. Our approach in which the usual conditions that are also used for the preparative purification of nanoparticles, no additives were necessary for the polymer coated nanoparticles with or without PEG modification.

V) FCS experiments

FCS was established by Madge et al. (1972) [26] as a way for measuring the diffusion constants of fluorescent particles dispersed in a solvent. From the diffusion constant of a particle it is possible to derive then its hydrodynamic radius through the Stokes-Einstein relation. Here, we first give a short overview of the FCS theory (details are discussed elsewhere [27-29]), and then we describe the experimental procedure for determining the average radius of the nanocrystals in the present work, using the FCS theory.

Let us assume that an excitation light source is focused on a tiny volume (V_{eff}) of the solution containing the fluorescent particles. On average, <N> particles will be sampled in this volume. However, the number of particles N(t) in this volume will fluctuate over time, because the particles can diffuse in and out of it. In the case of dilute solutions (so only few particles are present in the focus volume, on average), the fluctuation in the number of particles can be described by a Poisson distribution:

$$\sqrt{\frac{\langle (\delta N)^2 \rangle}{N}} = \frac{1}{\sqrt{N}} \tag{1}$$

$\delta N(t) = N(t) - <N>$ is the fluctuation of the number of particles, and $\langle N \rangle$ is the mean number of particles in the volume. Now, the concentration of the particles must be high enough to guarantee a good signal to noise ratio, but low enough to observe free particle diffusion. A good compromise would correspond roughly to 1 particle per femtoliter of the focus-volume V_{eff}. The FCS theory demonstrates that it is possible to derive the diffusion constant of the particles from $\delta N(t)$, and the principle can be understood in terms of a simple model. The time a particle needs to diffuse in and out of the focus volume depends indeed on its diffusion coefficient. The larger the diffusion coefficient, the faster the particles can diffuse in and out of the focus, and consequently faster time scale will characterize the fluctuations of the number of particles in V_{eff}. The analysis of the time scales involved in the fluctuations can be carried out by means of an autocorrelation function.

To a first approximation, we assume a constant value for the fluorescence emission from each particle inside the focus volume. In this simplified approach fluorescence fluctuations due to fluctuations in the absorption cross-section and in the quantum yield and blinking of the particles are neglected. Particles are also assumed to have a spherical shape.

The number of particles in the focus at a given time t can be experimentally determined by the total fluorescence F(t) collected. Since the excitation light is focused on a tiny volume V_{eff}, only the particles within this volume contribute to the fluorescence signal. The fluctuation $\delta F(t) = F(t) - <F>$ of the fluorescence signal is defined as the deviation from the mean fluorescence signal $\langle F \rangle$, which is given by:

$$\langle F \rangle = \frac{1}{T} \int_0^T F(t)dt \tag{2}$$

The number of particles N(t) in the focus can be written as an integral over the local particle concentration c($\underline{r}$, t):

$$N(t) = \int\limits_{V_{eff}} c(\underline{r},t)dV \tag{3}$$

We now assume that the fluctuations in the fluorescence signal are only due to local changes in the concentration $\delta c(\underline{r}, t)$ in the effective focus-volume V_{eff}. In addition, we merge the spatial parameters of the illumination to a function $W(\underline{r})$ that is written as:

$$W(\underline{r}) = e^{-2(x^2+y^2)/r_0^2} \cdot e^{-2z^2/z_0^2} \tag{4}$$

$W(r)$ is the so called Molecule Detection Efficiency which gives the probability of exciting and detecting a fluorescent particle in the solution. It is therefore the product of the excitation profile of the focused laser and the spatial collection efficiency of the confocal detection optics. Under carefully chosen setup conditions $W(\underline{r})$ can be approximated as a 3-dimensional Gaussian ellipsoid, as has been assumed in Equation (4). $\underline{r} = (x, y, z)$ describes the coordinates in the three-dimensional space. Here r_0 is the radius in the focal plane where the excitation intensity of the laser has dropped to $1/e^2$ compared to the center. The parameter z_0 gives the extension of the effective detection volume on the z-axis and is mainly determined by the used objective and the size of the pinhole.

The fluctuation of the fluorescence signal can then be written as:

$$\delta F(t) = \eta \int\limits_{V_{eff}} W(\underline{r}) \cdot \delta c(\underline{r},t)dV \tag{5}$$

The constant value η contains the quantum efficiency of the dye, detection efficiency and absorption cross-section. The normalized autocorrelation function $G(\tau)$ for fluorescence fluctuations $\delta F(t)$ is defined as:

$$G(\tau) = \frac{\langle \delta F(t) \cdot \delta F(t + \tau)\rangle}{\langle F(t)\rangle^2} \tag{6}$$

$G(\tau)$ is a measure of the self-similarity of the fluorescence signal after a delay-time τ. Thus $G(0)$ is the variance $<\delta F(t)^2>/<F>^2$. By inserting equation (5) in equation (6) the autocorrelation function becomes:

$$G(\tau) = \frac{\int\limits_{V}\int\limits_{V'} W(\underline{r}) \cdot W(\underline{r}') \cdot \langle \delta c(\underline{r},0) \cdot \delta c(\underline{r}', \hat{o})\rangle \, dVdV'}{\left(\langle c\rangle \int\limits_{V} W(\underline{r})dV\right)^2} \tag{7}$$

Under the assumption that the particles can diffuse freely in all three spatial directions (Brownian diffusion), we can derive an expression for the concentration fluctuations $\delta c(\underline{r},t)$ if we solve the diffusion equation, where D is the diffusion coefficient.

$$\frac{\delta c(\underline{r},t)}{\ddot{a}t} = D\nabla^2 \delta c(\underline{r},t) \tag{8}$$

We can use the following expression for $\delta c(\underline{r},t)$:

$$\delta c(\underline{r},t) = \delta c(\underline{r},0)\cdot e^{-\underline{r}^2/Dt} \tag{9}$$

The solution of the diffusion equation using (9) yields:

$$\langle \delta c(\underline{r},0)\delta c(\underline{r}',\tau)\rangle = \langle c\rangle \frac{1}{(4\pi D\tau)^{\frac{3}{2}}}\cdot e^{\frac{(\underline{r}-\underline{r}')^2}{4D\tau}} \tag{10}$$

Insertion of (10) into (7), followed by integration over the volume, finally leads to the autocorrelation function for freely diffusing particles (11).

$$G(\tau) = G_{\text{motion}}(\tau) = \frac{1}{V_{\text{eff}}\langle c\rangle}\cdot\frac{1}{(1+\frac{\tau}{\tau_D})}\cdot\frac{1}{\sqrt{1+\frac{\tau}{\tau_D\cdot s^2}}} \tag{11}$$

with the characteristic diffusion-time τ_D given by

$$\tau_D = \frac{r_0^2}{4D} \tag{12}$$

and the structure parameter s given by

$$s = \frac{z_0}{r_0} \tag{13}$$

The effective focus volume V_{eff} is then defined as

$$V_{\text{eff}} = \frac{\left(\int_V W(\underline{r})dV\right)^2}{\int_V W^2(\underline{r})dV} = \frac{\left(\int e^{-2\frac{x^2+y^2}{r_0^2}}\cdot e^{-2\frac{z^2}{z_0^2}}\,dV\right)^2}{\int e^{-4\frac{x^2+y^2}{r_0^2}}\cdot e^{-4\frac{z^2}{z_0^2}}\,dV} = \pi^{\frac{3}{2}}\cdot r_0^2\cdot z_0 \tag{14}$$

For fluorescent colloidal nanoparticles formula (11) has been proven to fit well to the experimental data[8]. For organic fluorophores a more advanced approach is applied: The correlation function G_{motion} (which describes only changes in fluorescence due to the motion of

---

[8] In our first manuscript (7) we have used Formula (16) also to fit the autocorrelation functions of CdSe/ZnS. However, in the following manuscript (30) we have used Formula (11) to the autocorrelation functions of CdSe/ZnS, since they described the results better. Also in this manuscript we use (11) to fit the autocorrelation functions of CdSe/ZnS. For organic fluorophores the more complex Formula (16) has to be applied.

the particles) is therefore multiplied by a kinetic factor that accounts for blinking / flickering [29,31] in the fluorescence of the particles

$$X_{triplet} = \frac{1 - T_{trip} + T_{trip} \cdot \exp\dfrac{\hat{o}}{\hat{o}_{trip}}}{1 - T_{trip}} \; .$$

(15)

The entire fit function than reads

$$G(\tau) = 1 + X_{triplet}\, G(\tau)$$

(16)

For measurements involving CdSe/ZnS quantum dots only the simple approach (11) was used, for measurement of organic fluorophore approach (16).

The hydrodynamic radius r_h of the spherical particles can be obtained by inserting the diffusion constant D (from equation (12)) into the Stokes-Einstein-equation:

$$r_h = \frac{kT}{6\pi\eta D}$$

(17)

In our work we define the effective diameter d_{eff} of nanoparticle conjugates as two times their measured hydrodynamic radius:

$$d_{eff(FCS)} = 2 \cdot r_h$$

(18)

Having given a brief overview of the FCS theory, we now describe the experimental procedure followed for the determination of the average diameter of the polymer coated nanocrystals synthesized in the present work.

Figure SI-V.1 shows a sketch of the experimental setup. A laser beam is focused by an objective with a high numerical aperture. Fluorescent light that is collected by the same objective can pass through the dichroic mirror as it is slightly shifted to higher wavelengths compared to the excitation. A 50/50 beamsplitter gives half of the intensity to two independent detection channels. With the filters the desired detection wavelengths can be chosen. Behind the pinholes of variable size the photons are detected with avalanche photodiodes giving the intensity versus time F(t). An autocorrelation of the signal is done by a correlator card attached to a computer.

The Experiments were performed with a Confocor2 FCS-setup from Zeiss™. The laser light from a HeNe-Laser (Lasos/Zeiss, 633 nm wavelength) was coupled into the system via a dichroic mirror and was focused with a Zeiss C-Apochromat water immersion objective (40x; numerical aperture: 1.2) to a small volume within the diluted sample. The fluorescence signal emitted from the particles passed through a dichroic mirror and the focal plane was selected by a pinhole with 90 µm diameter. The signal was split by a 50/50 beamsplitter and collected by two Avalanche Photo Diodes (after passing appropriate filters).
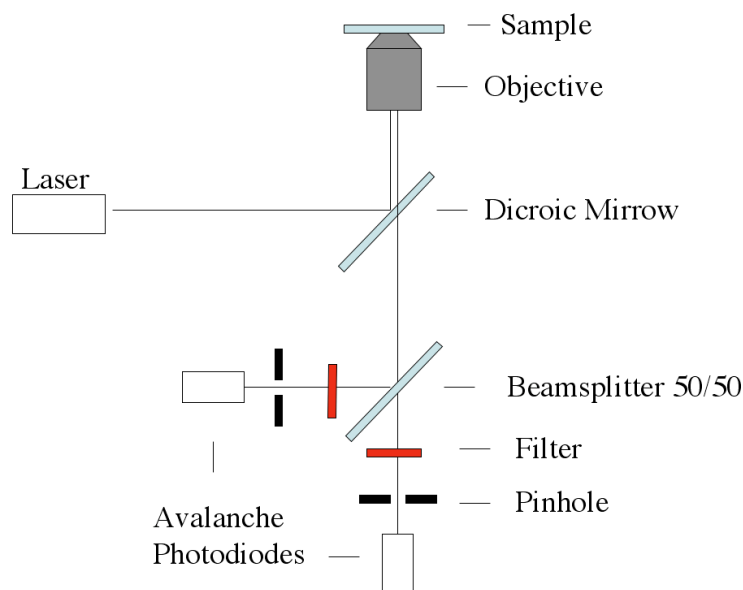
Figure SI-V.1: FCS setup. An Ar-ion-Laser (Lasos/Zeiss) was used, the cut-off wavelength of the dicroic mirror was 510 nm, and 510 nm longpass filters were used to observe the emitted fluorescence.

First of all, the system had to be calibrated. In particular the volume of the focus had to be determined experimentally. For this purpose fluorescent molecules with a known diffusion constant were used as calibration sample. We used a solution of Cy5 dye (Molecular Probes, excitation maximum 649 nm, emission maximum 670 nm) dissolved in water (10 nM concentration), as this dye has a fluorescence in the red similar to the CdSe/ZnS nanoparticles that are investigated in this study. The time trace of the fluorescence signal $F(t)$ from this sample was recorded 10 times, each time for 20 seconds (Figure SI-V.2). For each measurement, the autocorrelation function $G(\tau)$ for the fluorescence fluctuations $\delta F(t)$ was calculated by using equation (6) (Figure SI-V.3). The experimental data for the autocorrelation function were fitted with equation (16), using the 5 fit parameters τ_{trip}, T_{trip}, τ_D, s, and $<N> = V_{eff}<c>$. Since the diffusion constant for Cy5 is known ($D = 250$ $\mu m^2/s$), the focal radius r_0 could be derived via (12) using for τ_D the value obtained from the fit. Similarly, z_0 could be derived via (13) by using the fit results for the structure parameter s and r_0. The mean values for r_0 and z_0 (and thus also for s) obtained from the ten individual measurements where then used for all the measurements on CdSe/ZnS nanocrystal samples.
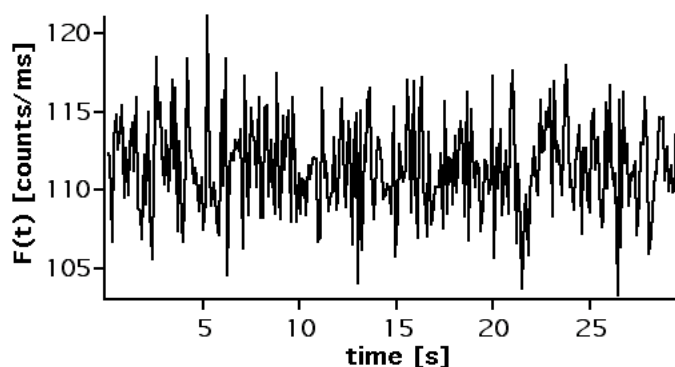

Figure SI-V.2: Time trace of the recorded fluorescence intensity F(t) of a Cy5 fluorescent dye solution.
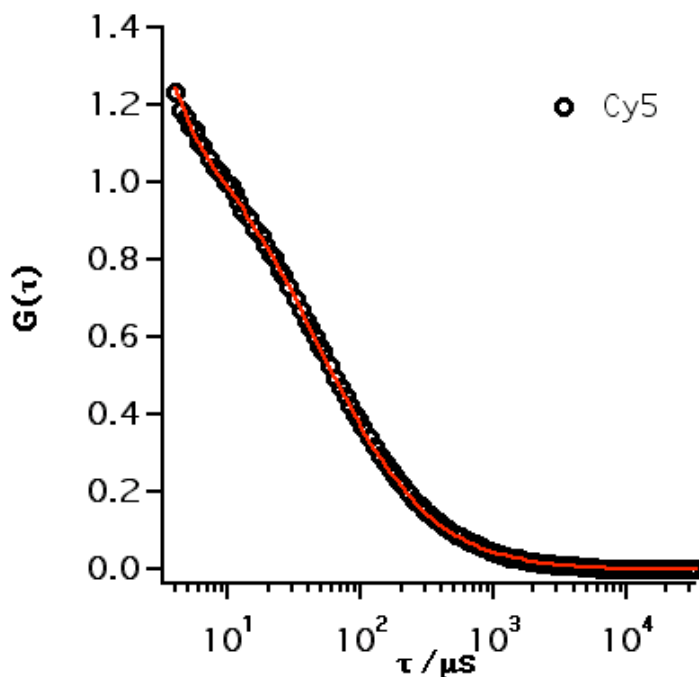
Figure SI-V.3: *Autocorrelation function G(τ) calculated from the F(t) data shown in Figure SI-V.2 (dotted line). The curve was fitted with the function given in equation (16). The fit yielded the five fit parameters: Triplet time τ_{trip} = 3 μs, a triplet fraction of 11% (T_{trip} = 0.11), the characteristic diffusion time τ_D = 46 μs, structure parameter s = 8, and average number of dye molecules within the focal volume <N> = V_{eff}<c> = 0.85. The focal radius r_0 was calculated by means of (12), using the known diffusion-constant of Cy5 (D = 250 μm²/s), and was equal to 215 nm.*

For the measurements on the nanocrystal samples, nanocrystal solutions with a concentration of approximately 50 nM were deposited on a coverslip over the objective (the same as for the Cy5 dye solution). The time trace of the fluorescence signal F(t) was recorded at least ten times, each time for 20 seconds. The corresponding autocorrelation functions G(τ) were calculated using equation (6) and were fitted with (11). This time only two fit parameters were used: τ_D and <N> = V_{eff}<c>. The geometrical parameters for the focus volume (r_0 and z_0, as well as s) where in fact known from the previous calibration with the Cy5 solution. The diffusion constant for the nanocrystals D could be calculated via (12), using the diffusion time τ_D, as determined from the fit, and the known focal radius r_0. Finally, the hydrodynamic radius of the nanocrystals was calculated using the Stokes-Einstein-equation (17). As viscosity of water η_{water} = 0.98 mPa·s respectively was assumed at 20 °C. At least 10 individual measurements were performed for each sample, and the resulting hydrodynamic radius was determined as the mean value of the measurements.

In Figures SI-V.5 and SI-V.6 the correlation functions that have been determined in this work for different CdSe/ZnS - PEG conjugates are shown. The effective diameters derived from the fits are presented in the main text of this manuscript.
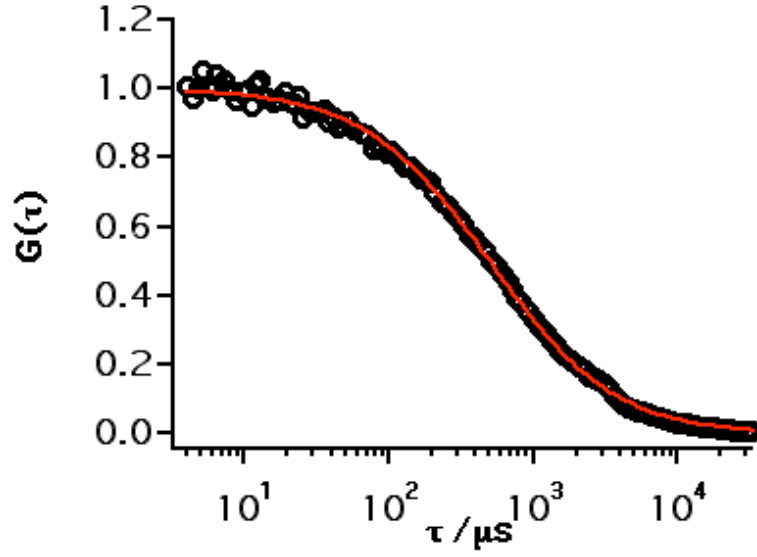
Figure SI-V.4: *Autocorrelation function G(τ) calculated from the F(t) data recorded on a sample of red fluorescent, polymer-coated CdSe/ZnS nanocrystals dissolved in water (dotted line). The curve was fitted with the function given in equation (11), whereby the structure parameter (as determined from the calibration with Cy5) was kept fixed at s = 8. The fit yielded the following the characteristic diffusion time τ_D = 524 μs. With the known value for r_0 =215 nm the diffusion constant was determined via (12) to be D = 22 μm²/s. According to the Stokes-Einstein relation this corresponds to a hydrodynamic radius of r_h = 11.3 nm.*

Figure SI-V.5: *Correlation functions (experimental data: black points; fits: red lines) for polymer coated CdSe/ZnS nanoparticles that have been saturated with PEG molecules of different molecular weight.*
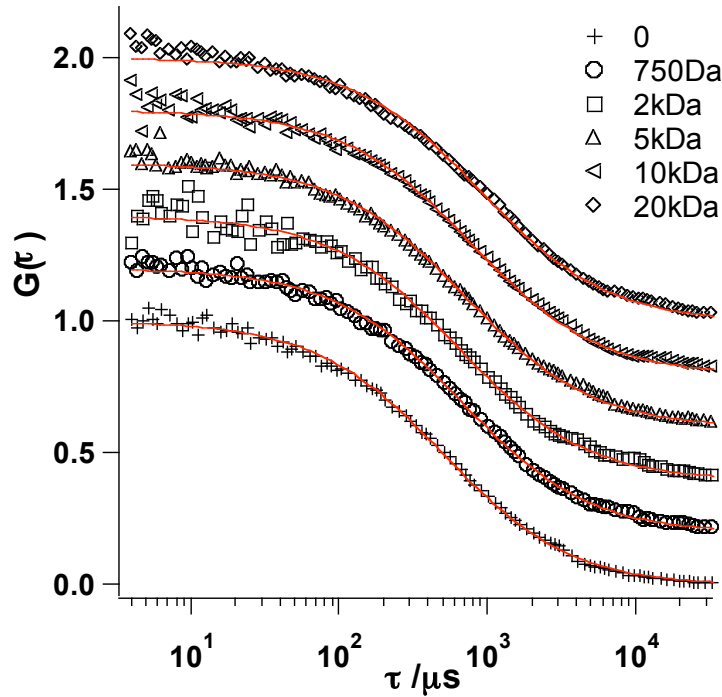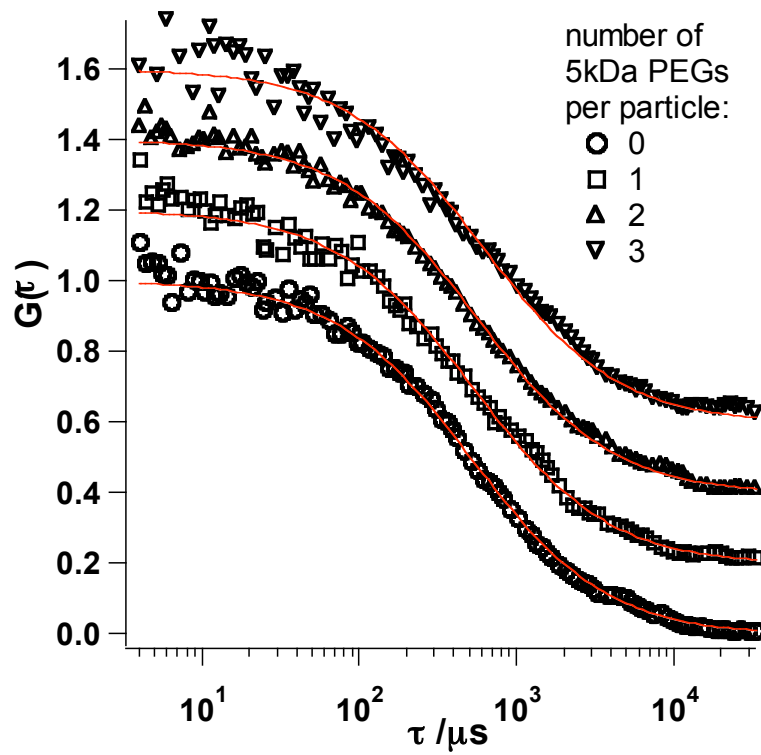
Figure SI-V.6: Correlation functions (experimental data: black points; fits: red lines) for polymer coated CdSe/ZnS nanoparticles that have been modified with 0, 1, 2, 3 PEG molecules per particle. The PEG had a molecular weight of 5 kDa.

VI) Thermophoresis experiments

Introduction: Thermophoresis, also named Soret Effect, is known for 150 years and describes the movement of molecules in temperature gradients, which is usually observed from hot to cold. A general theoretical description for behavior of molecules in solution was missing until recently [32]. With our method we create strong temperature gradients on the micron scale by infrared laser heating. A measure for the magnitude of the thermophoretic effect is the Soret coefficient S_T. It can be obtained from the steady state profile at constant laser heating typically after 100 seconds for the given geometry and diffusion coefficient. Given the temperature at radius r obtained from temperature dependent fluorescence, the concentration of fluorescent particles c(r) can be fitted with the steady state thermophoretic profile given by

$$c(r) = c_0 e^{-S_T(T(r)-T_0)} \tag{1}$$

with the chamber temperature T_0 and the bulk particle concentration c_0. Since S_T relates the concentration change exponentially to the temperature difference in principal very strong depletion can be expected at small temperature increase. If local equilibrium condition holds [33], the Soret coefficient is related to the solvation entropy ΔS by the expression

$$S_T = -\Delta S / kT \tag{2}$$

The build-up of a concentration gradient and the steady state are used to obtain important parameters of the fluorescent particles like effective charge and entropy of solvation [32]. Two contributions dominate the particle entropy S in water: the entropy of ionic shielding and the temperature sensitive entropy of water hydration. The interplay of these quantities determines whether particles move from hot to cold or vice versa. In some cases a balance of certain surface modifications may cancel out any thermophoretic motion. An important application has been established to obtain particle sizes by measuring the diffusion coefficients as described in the following.

Detecting molecules / particles: The technique is based on fluorescence microscopy were imaging was provided with an AxioTech Vario fluorescence microscope (Zeiss), illuminated with a high power LED (Luxeon) or Xenon-lamp (XBO, Osram) and imaged with the CCD Camera SensiCamQE (PCO). The filter sets allowed for a fluorescence excitation between 450 and 500 nm, while emission was detected at wavelengths > 560 nm. Nanoparticle concentration was inferred from fluorescence images, that were measured with a 40 x oil objective (NA =1.3). This relates to a field of view of 200 x 200 μm.
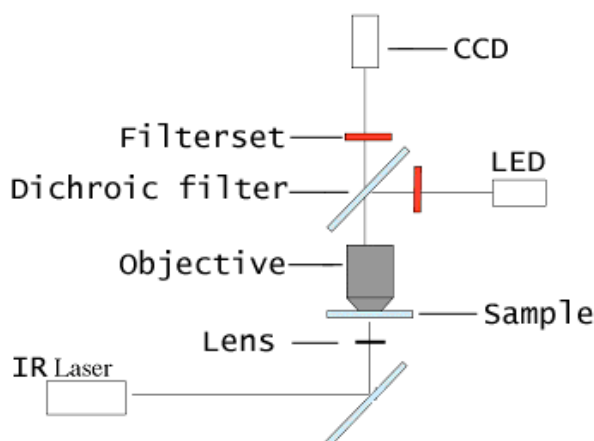
Figure SI-VI.1: Experimental Setup. An IR laser is coupled into a aqueous sample from below. Fluorescence excitation is provided by LED illumination and imaging is performed by a CCD camera device.

Manipulating molecules / particles: Thermophoresis is an all optical method to manipulate even small molecules / particles in solution. A localized temperature distribution is created in aqueous solution by means of infrared laser heating and particles move (typically to colder regions) to maximize their entropy of solvation. The velocity of the movement and the respective steady state, were thermodiffusion is balanced by backdiffusion, are strongly dependent on particle properties like charge and size. The temperature gradients used to induce thermodiffusive motions were created by aqueous absorption of an infrared laser at 1480 nm wavelength and a maximum power of 320 mW (Furukawa). Water strongly absorbs at this wavelength with an attenuation length of $\kappa = 320 \ \mu m$. The laser beam was moderately focused with a lens of 8 mm focal distance (Thorlabs, C240TM-C). Typically, the temperature in the solution was raised by 2 - 15 K in the beam center. The laser was focused into the sample from below the sample holder and the beam position in the x/y plane could be adjusted by two galvanoometrically controlled infrared mirrors (Cambridge Technology 6200-XY Scanner with Driver 67120).

Temperature calibration: Temperatures have been measured with the temperature dependent fluorescence signal of the dye BCECF, diluted to 50 µM in 10 mM TRIS buffer. Details of bleaching correction and temperature extraction were described previously[34]. From the total temperature dependence of BCECF of -2.8 %/K, only -1.3 % /K stems from pH drift of the used TRIS buffer. The remaining -1.5 % /K are the result of thermodiffusion of the dye itself, measured to be $S_T = 0.015$ /K with the concentration over time method described below. Determining the exact temperature distribution is important to quantify the thermophoretic effect, but not necessary to measure diffusion of particles [34].

Measurement: Measurements were performed in thin microfluidic chambers of 20 µm in height. A droplet of 1.8µl was sandwiched between an object slide and cover slide (Roth, Karlsruhe). To avoid evaporation the chamber was sealed with nail polish. Beside the low consumption of sample volume the low sample thickness provides several advantages. Convection is largely suppressed by this geometry and the sample is homogeneously heated throughout its height since only a fraction of the laser power is absorbed on this lengthscale. Diffusion constants and the respective radii are measured as described in the following. The

sample was illuminated and fluorescence was recorded without heating with a frequency up to 20 Hz, depending on the fluorescence intensity. This determined the 100 % relative concentration level. Then the laser was turned on, and immediately the concentration in the heated center decreased until steady state was reached. The laser was turned off and images were recorded until the established concentration gradient had relaxed completely. Please note that thermal relaxation is much faster and established before 100 ms. For the sizes measured throughout this work a typical experiment was performed within 10 s. We obtained the diffusion constant D by analyzing the flattening of the concentration profile over time after turning the infrared laser beam off. First we calculated radial concentration averages, since we had heated with a round symmetric heatspot. The concentration profile obtained after thermal relaxation (> 100 ms) was fitted polynomically. The fit is the starting point to calculate the backdiffusion in a one dimensional finite element model in radial coordinates (FEMLab, Comsol) over time. The experimentally measured radial concentration timecourse was fitted by adjusting the diffusion coefficient used in the numerical calculation. The hydrodynamic particle radius r_h has been calculated by using the Einstein relation

$$D = kT / \pi \eta r_h \qquad (3)$$

In contrast to the gel electrophoresis and size exclusion chromatography measurements the effective diameters $d_{eff} = 2 \cdot r_h$ obtained with thermophoresis measurements do not depend on a comparison with standard samples of known diameter, but are absolute values. Since the Au-PEG conjugates do not fluoresce they could not be analyzed with thermophoresis. The measurement is also not sensitive to impurities even though they may be fluorescent. In Table VI.1 some results are listed.

sample	D [m^2/s]	r_h [nm]
QD655 carboxyl	$3.0 \cdot 10^{-11}$	7.0 ± 1.0
QD655 SA	$1.6 \cdot 10^{-11}$	12.8 ± 1.0
λ-DNA	$6.0 \cdot 10^{-13}$	348 ± 3.0

Table SI-VI.1: Nanoparticles investigated with thermophoresis. Enlisted are the diffusion constants D and the hydrodynamic radii r_h. The samples are the same as in Tables SI-IV.1 and SI-IV.2.

VII) Comparison of different methods

VII.1) Introduction to the differences of the methods

The most straight-forward way to determine the size of a particle is to make an image of the particle from which the size can be directly obtained. Due to their small size **optical microscopy** is obviously not suitable for this purpose due to the lateral resolution which is limited by diffraction. When electron- instead of light waves are used the resolution is increased by orders of magnitudes and thus individual single nanoparticles can be imaged with **transmission electron microscopy** (TEM). However, the contrast of the inorganic core is much higher than that of its organic shell. Therefore, in most cases only the inorganic particle core can be seen on a TEM image and it is not possible to directly measure the effective total particle diameter, although exceptions exist as for example for relatively thick silica layers around an inorganic particle core [35]. When TEM grids are prepared with the appropriate concentration of nanoparticles, the particles can self-assemble to 2-dimensional lattices [36]. In this way the size of the surfactant layer can be estimated as two times the minimum distance between the two adjacent inorganic particle cores [6,37]. For TEM imaging particles have to be deposited on a substrate and the solution in which the particles are dispersed must be evaporated. The thickness of the organic layer is likely to be underestimated due to the drying procedure. It is known for example that the organic layers of two adjacent particles can intercalate [6,37]. In **atomic force microscopy** (AFM) the surface of a substrate is probed with a tiny cantilever-tip and the deflection of the tip is a measure for the height profile of the sample. In this way the height of individual nanoparticles that are adsorbed on a substrate can be measured [38] and even the attachment of biological molecules can be analyzed [39,40]. Although nanoparticles have to be attached to a substrate, measurements can in principle be performed in solution. The measured height of the particles is a direct equivalent for their effective diameter. Due to the lateral resolution of the AFM which is limited by the sharpness of the probing tip, information about the effective diameter cannot be taken from the image of the surface but must be derived from the height profile. Potential problems include compression of the soft organic shell around the hard inorganic particle core which leads to too small effective diameters, although this problem can be reduced when the AFM is operated in tapping mode. Electrostatic and other interactions between the tip and the particle can also lead to wrong effective diameters [41]. AFM is an effective but also laborious method (if statistics have to be obtained) for directly measuring the effective diameter of single particles [38].

In contrast to the above described imaging methods the size of nanoparticles can also be determined by size-selective sorting. With **size exclusion chromatography** (SEC) nanoparticles can be sorted by size with size exclusion columns [18-25,42-45]. Size exclusion columns comprise a porous gel matrix through which the particles are run by the flow of the mobile phase. Smaller particles can diffuse into the pores and are therefore eluted later than bigger particles. By using particles with known size (such as protein calibration standards) a calibration curve between the elution time versus the effective particle size can be obtained [12, Holtzhauer, 1992 #10875]. By running a sample of nanoparticles through the same size exclusion column and by measuring the elution time the effective diameter of the particles can be interpolated from the calibration curve [24,25]. Size determination with SEC is an ensemble measurement. Although the particles are dispersed in their natural solvent the analysis relies on a stationary phase, i.e. a gel matrix, and the effective diameter of the particles can be influenced by interactions with the gel which can lead to non-ideal effects, e.g. the retardation of the sample by electrostatic or hydrophilic-hydrophobic interactions. Another size-selective sorting technique is **gel electrophoresis**. Here charged particles are run through a gel matrix by

applying an electric field along the gel. The bigger the particles are the slower they migrate on the gel and the smaller their electrophoretic mobility is [10,40,44,46-50]. Analogous to SEC, particles with known diameter can be run on the gel which can be used to generate a calibration curve that relates the electrophoretic mobility of particles to their effective diameter. In this way the effective diameter of particles can be determined by measuring their electrophoretic mobility. Of course the electrophoretic mobility of particles also depends on their charge and therefore size-selective sorting by gel electrophoresis can only be used for particles with similar surface charge. Like SEC, gel electrophoresis is an ensemble measurement in which the particles are dispersed in their solvent. However, interactions with the gel matrix, such as squeezing of the soft organic shell around the hard inorganic particle core, can lead to errors in the determination of the effective particle diameter. Particle sorting can also be achieved by free flow **capillary electrophoresis** (CE) without involving a gel matrix [51,52]. However, the resolution of the sorting usually decreases without gel matrix.

The size of particles can be derived from their diffusion coefficient via the Stokes-Einstein-relation. Diffusion coefficients of particles dispersed in a solvent can be experimentally determined with several techniques. In all this methods particles can be freely dispersed in the solvent without the need for a gel matrix or substrate to be attached to the particles. With **dynamic light scattering** (DLS) fluctuations in the light that has been scattered from a particle solution are analyzed by calculating the autocorrelation function [45,50,53-58]. The diffusion constant can be directly derived as absolute value from the correlation function with an analytical model for free diffusion. Quantitative analysis is hampered by the hybrid nature of the nanoparticles, whose refraction index of the inner inorganic core is significantly different from the refraction index of their organic shell. This complicates the transformation of the measured intensity distribution to a number distribution of particles size. Whereas light scattering works with relatively concentrated samples, **fluorescence correlation spectroscopy** (FCS) [26-29] measures the fluorescence of particles in a very diluted solution, in such way that on average there is always only one particle in the focal volume of a confocal fluorescence microscope. By this means, the signal of the recorded fluorescence reflects the light fluctuations caused by particles diffusing through the gaussian excitation profile of a focused laser. The mean diffusion constant of the particles is derived from the autocorrelation function of the intensity fluctuations of the recorded fluorescence [7,30,59-62]. In a simplified picture, a particle with a smaller diffusion coefficient that is moving with Brownian motion, remains longer in the focus of the excitation light and therefore fluctuations of the recorded intensity will be found on a slower time scale which is derived by the decay of the autocorrelation function of the measured intensity signal. The effective size of the particles is then again derived by the Stokes-Einstein-relation. Since the volume of the excitation focus is not known initially, it has to be determined by means of a dye with a known diffusion constant. In **thermophoresis** a solution that contains dispersed fluorescent particles is locally heated with an IR laser. Due to the heat gradient particles move into or out of the heated area. The direction of motion depends on the surface properties of the particle. The heat gradient results in an inhomogeneous concentration distribution imaged by fluorescence microscopy. After the heat source is removed the system equilibrates by diffusion and the fluorescence distribution becomes again homogeneous. By recording the changes in concentration the mean diffusion coefficient of the particle ensemble can be determined [32-34].

We also have to mention other methods that were not employed in this study, such as **X-ray diffraction** (XRD) [63,64], small angle scattering with x-rays (**small angle x-ray scattering**, SAXS) [63] and neutrons (**small angle neutron scattering**, SANS) [65]. Whereas XRD is insensitive to organic shells around the inorganic particle core, small angle scattering is

sensitive to it. However, it is very complicated to extract quantitative data for inhomogeneous systems, which are composed of various organic layers with inhomogeneous thickness, since numbers only can be obtained via fitting the data with layer-models. Furthermore, particles can be separated by their effective diameter by **analytical centrifugation** [55,66,67]. While this method yields good results for particles with a homogeneous mass density, in the case of core-shell nanoparticles the average mass density changes with the thickness of the (organic) shell, which complicates the calibration of the density gradient and a quantitative evaluation of particle size distributions. A summary of all the methods is shown in Table SI-VII.1.

Method	Limited to nanoparticles that are	Particle state during measurement
Fluorescence correlation spectroscopy (FCS)	fluorescent	in solution
Thermophoresis	fluorescent	in solution
Dynamic light scattering (DLS)		in solution
Gel electrophoresis	charged	in solution (gel)
Size exclusion chromatography (SEC)		in solution (gel)
Capillary electrophoresis (CE)	charged	in solution (free or gel)
Analytical centrifugation		in solution (density gradient)
Transmission electron microscopy (TEM)	composed out of atoms with high numbers Z of nucleons	on surface (dry)
Atomic force microscopy (AFM)		on surface (wet or dry)
X-ray diffraction (XRD)	crystalline	powder
Small-angle X-ray or neutron scattering (SAXS, SANS)		in solution

Table SI-VII.1: Overview and classification of analytical methods for determining nanoparticle diameters in respect to nanoparticle type and state.

VII.2) Comparison of our results with values from literature

Though several studies exist in which the effective diameters of particles have been measured most of these studies are either based on only one method or only one type of particle surface. The groups of Mattoussi [50] and Nie [58] have reported extensive studies in which data obtained with DLS and gel electrophoresis [50], and particles with different surface modification [58] were compared. As particles with different surface modification were used in these studies we cannot directly compare these values with those we obtained in our present study. Pons et al. determined an effective diameter of about 14.2 nm for polymer-coated CdSe/ZnS particles with fluorescence at 565 nm, as well with gel electrophoresis as with DLS, whereby their polymer-coating procedure was not exactly the same as the one we used for our study [50]. This lies in the same range as we determined with several methods for our plain polymer-coated CdSe/ZnS particles (cfg. Tables 2 and 3 of the main paper), though our particle cores were slightly larger (fluorescence at 625 nm). Very recently, Yu et al. have published SEC and DLS data [68] of polymer-coated nanoparticles modified with PEG. Their diameters are in good agreement with our data, but slightly larger. This could be due to the longer sidechains of the polymer (octadecene instead of tetradecene). For a meaningful comparison of the thickness of both polymer and PEG shell with our results, data from particles coated with the plain polymer would be helpful. A specialized review about the size characterization of colloidal nanoparticles could be helpful to researchers to get a more complete overview of work that has already been done by others.

VIII) References

(1)   Reiss, P.; Bleuse, J.; Pron, A. *Nanoletters* 2002, *2*, 781.

(2)   Kudera, S.; Zanella, M.; Giannini, C.; Rizzo, A.; Li, Y.; Gigli, G.; Cingolani, R.; Ciccarella, G.; Spahl, W.; Parak, W. J.; Manna, L. *Advanced Materials* 2007, *19*, 548.

(3)   Dabbousi, B. O.; Rodriguez-Viejo, J.; Mikulec, F. V.; Heine, J. R.; Mattoussi, H.; Ober, R.; Jensen, K. F.; Bawendi, M. G. *Journal of Physical Chemistry B* 1997, *101*, 9463.

(4)   Yu, W. W.; Wang, Y. A.; Peng, X. *Chemistry of Materials* 2003, *15*, 4300.

(5)   Brust, M.; Walker, M.; Bethell, D.; Schiffrin, D. J.; Whyman, R. *J. Chem. Soc., Chem. Commun.* 1994, *1994*, 801.

(6)   Fink, J.; Kiely, C. J.; Bethell, D.; Schiffrin, D. J. *Chemistry of Materials* 1998, *10*, 922.

(7)   Pellegrino, T.; Manna, L.; Kudera, S.; Liedl, T.; Koktysh, D.; Rogach, A. L.; Keller, S.; Rädler, J.; Natile, G.; Parak, W. J. *Nanoletters* 2004, *4*, 703.

(8)   Sperling, R. A.; Pellegrino, T.; Li, J. K.; Chang, W. H.; Parak, W. J. *Advanced Functional Materials* 2006, *16*, 943.

(9)   Yu, W. W.; Qu, L.; Guo, W.; Peng, X. *Chemistry of Materials* 2003, *15*, 2854.

(10)   Pellegrino, T.; Sperling, R. A.; Alivisatos, A. P.; Parak, W. J. *Journal of Biomedicine and Biotechnology* 2007, *submitted*.

(11)   Sartori, R.; Sepulveda, L.; Quina, F.; Lissi, E.; Abuin, E. *Macromolecules* 1990, *23*, 3878.

(12)   Kuga, S. *Journal of Chromatography A* 1981, *206*, 449.

(13)   Holtzhauer, M.; Rudolph, M. *Journal of Chromatography A* 1992, *605*, 193.

(14)   Grubisic, Z.; Rempp, P.; Benoit, H. *Journal Of Polymer Science Part B-Polymer Letters* 1967, *5*, 753.

(15)   Hagel, L. Gel Filtration. In *Protein Purification. Principles, High Resolution Methods and Applications*; 2 ed.; Janson, J.-C., Ryden, L., Eds.; John Wiley & Sons: New York, 1998.

(16)   Fee, C. J.; Alstine, J. M. V. *Bioconjugate Chemistry* 2004, *15*, 1304.

(17)   Dubin, P. L.; Edwards, S. L.; Mehta, M. S.; Tomalia, D. *Journal of Chromatography* 1993, *635*, 51.

(18)   Siebrands, T.; Giersig, M.; Mulvaney, P.; Fischer, C.-H. *Langmuir* 1993, *9*, 2297.

(19)   Fischer, C.-H.; Giersig, M.; Siebrands, T. *Journal of Chromatography A* 1994, *670*, 89.

(20)   Fischer, C.-H.; Kenndler, E. *Journal of Chromatography A* 1997, *773*, 179.

(21)   Wei, G.-T.; Liu, F.-K. *Journal of Chromatography A* 1999, *836*, 253–260.

(22)   Wei, G.-T.; Liu, F.-K.; Wang, C. R. C. *Analytical Chemistry* 1999, *71*, 2085.

(23)   Jimenez, V. L.; Leopold, M. C.; Mazzitelli, C.; Jorgenson, J. W.; Murray, R. W. *Analytical Chemistry* 2003, *75*, 199.

(24)   Al-Somali, A. M.; Krueger, K. M.; Falkner, J. C.; Colvin, V. L. *Analytical Chemistry* 2004, *76*, 5903.

(25)   Krueger, K. M.; Al-Somali, A. M.; Falkner, J. C.; Colvin, V. L. *Analytical Chemistry* 2005, *77*, 3511.

(26)   Magde, D.; Elson, E.; Webb, W. W. *Physical Review Letters* 1972, *29*, 705.

(27)   Eigen, M.; Rigler, R. *Proc. Natl. Acad. Sci. USA* 1994, *91*, 5740.

(28)   Schwille, P.; Bieschke, J.; Oehlenschläger, F. *Biophysical Chemistry* 1997, *66*, 211.

(29)   Krichevsky, O.; Bonnet, G. *Rep. Prog. Phys.* 2002, *65*, 251.

(30)   Liedl, T.; Keller, S.; Simmel, F. C.; Rädler, J. O.; Parak, W. J. *Small* 2005, *1*, 997.

(31)   Amediek, A.; Haustein, E.; Scherfeld, D.; Schwille, P. *Single Molecules* 2002, *3*, 201.

(32)   Duhr, S.; Braun, D. *PNAS* 2006, *103*, 19678.

(33)   Duhr, S.; Braun, D. *Physical Review Letters* 2006, *96*, 168301.

(34)   Duhr, S.; Arduini, S.; Braun, D. *European Physical Journal E* 2004, *15*, 277.

(35)   Kobayashi, Y.; Horie, M.; Konno, M.; Rodriguez-Gonzalez, B.; Liz-Marzan, L. M. *J. Phys. Chem. B* 2003, *107*, 7420.

(36)   Zanchet, D.; Moreno, M. S.; Ugarte, D. *Physical Review Letters* 1999, *82*, 5277.

(37)   Yonezawa, T.; Onoue, S.-y.; Kimizuka, N. *Langmuir* 2001, *17*, 2291.

(38)   Gerion, D.; Pinaud, F.; Williams, S. C.; Parak, W. J.; Zanchet, D.; Weiss, S.; Alivisatos, A. P. *Journal of Physical Chemistry B* 2001, *105*, 8861.

(39)   Cai, W.; Shin, D.-W.; Chen, K.; Gheysens, O.; Cao, Q.; Wang, S. X.; Gambhir, S. S.; Chen, X. *Nano Letters* 2006, *6*, 669.

(40)   Nehilla, B. J.; Vu, T. Q.; Desai, T. A. *Journal of Physical Chemistry B* 2005, *109*, 20724.

(41)   Ebenstein, Y.; Nahum, E.; Banin, U. *Nanoletters* 2002, *2*, 945.

(42)   Fischer, C.-H.; Lilie, J.; Weller, H.; Katsikas, L.; Henglein, A. *Ber. Bunsenges. Phys. Chem.* 1989, *93*, 61.

(43)   Fischer, C.-H.; Weller, H.; Katsikas, L.; Henglein, A. *Langmuir* 1989, *5*, 429.

(44)   Pinaud, F.; King, D.; Moore, H.-P.; Weiss, S. *Journal of the American Chemical Society* 2004, *126*, 6115.

(45)   Wilcoxon, J. P.; Provencio, P. P. *Journal of Physical Chemistry B* 2005, *109*, 13461.

(46)   Eychmüller, A.; Katsikas, L.; Weller, H. *Langmuir* 1990, *6*, 1605.

(47)   Zanchet, D.; Micheel, C. M.; Parak, W. J.; Gerion, D.; Alivisatos, A. P. *Nanoletters* 2001, *1*, 32.

(48)   Parak, W. J.; Pellegrino, T.; Micheel, C. M.; Gerion, D.; Williams, S. C.; Alivisatos, A. P. *Nanoletters* 2003, *3*, 33.

(49)   Song, X.; Li, L.; Qian, H.; Fang, N.; Ren, J. *Electrophoresis* 2006, *27*, 1341.

(50)   Pons, T.; Uyeda, H. T.; Medintz, I. L.; Mattoussi, H. *Journal Of Physical Chemistry B* 2006, *110*, 20308.

(51)   Peterson, R. R.; Cliffel, D. E. *Analytical Chemistry* 2005, *77*, 4348.

(52)   Bücking, W.; Nann, T. *IEE proceedings - Nanobiotechnology* 2006, *153*, 47.

(53)   Cardenas, M.; Schillen, K.; Nylander, T.; Jansson, J.; Lindman, B. *Physical Chemistry Chemical Physics* 2004, *6*, 1603.

(54)   Cardenas, M.; Schillen, K.; Pebalk, D.; Nylander, T.; Lindman, B. *Biomacromolecules* 2005, *6*, 832.

(55)   Luccardini, C.; Tribet, C.; Vial, F.; Marchi-Artzner, V.; Dahan, M. *Langmuir* 2006, *22*, 2304.

(56)   Jiang, W.; Mardyani, S.; Fischer, H.; Chan, W. C. W. *Chemistry of Materials* 2006, *18*, 872.

(57)   Ipe, B. I.; Shukla, A.; Lu, H.; Zou, B.; Rehage, H.; Niemeyer, C. M. *ChemPhysChem* 2006, *7*, 1112.

(58)   Smith, A. M.; Duan, H.; Rhyner, M. N.; Ruan, G.; Nie, S. *Phys. Chem. Chem. Phys.* 2006, *8*, 3895.

(59)   Zhang, P.; Li, L.; Dong, C.; Qian, H.; Ren, J. *Analytica Chimica Acta* 2005, *546*, 46.

(60)   Doose, S.; Tsay, J. M.; Pinaud, F.; Weiss, S. *Anal. Chem.* 2005, *77*, 2235.

(61)   Dong, C.; Bi, R.; Qian, H.; Li, L.; Ren, J. *SMALL* 2006, *2*, 534.

(62)   Jin, T.; Fujii, F.; Yamada, E.; Nodasaka, Y.; Kinjo, M. *Journal of the American Chemical Society* 2006, *128*, 9288.

(63)   Borchert, H.; Shevchenko, E. V.; Robert, A.; Mekis, I.; Kornowski, A.; Grübel, G.; Weller, H. *Langmuir* 2005, *21*, 1931.

(64)   Petkov, V.; Peng, Y.; Williams, G.; Huang, B.; Tomalia, D.; Ren, Y. *PHYSICAL REVIEW B* 2005, *72*, 195402.

(65)   Zackrisson, M.; Stradner, A.; Schurtenberger, P.; Bergenholtz, J. *Langmuir* 2005, *21*, 10835.

(66)   Calabretta, M.; Jamison, J. A.; Falkner, J. C.; Liu, Y. P.; Yuhas, B. D.; Matthews, K. S.; Colvin, V. L. *Nano Letters* 2005, *5*, 963.

(67)   Slocik, J. M.; Stone, M. O.; Naik, R. R. *Small* 2005, *1*, 1048.

(68)   Yu, W. W.; Chang, E.; Falkner, J. C.; Zhang, J.; Al-Somali, A. M.; Sayes, C. M.; Johns, J.; Drezek, R.; Colvin, V. L. *J. Am. Chem. Soc.* 2007, *129*, 2871.